

Dynamic structure selection and instabilities of driven Josephson lattice in high-temperature superconductors

A. E. Koshelev and I. Aranson

Materials Science Division, Argonne National Laboratory, Argonne, Illinois 60439

(October 25, 2018)

We investigate the dynamics of the Josephson vortex lattice in layered high- T_c superconductors at high magnetic fields. Starting from coupled equations for superconducting phases and magnetic field we derive equations for the relative displacements [phase shifts] between the planar Josephson arrays in the layers. These equations reveal two families of steady-state solutions: lattices with constant phase shifts between neighboring layers, starting from zero for a rectangular configuration to π for a triangular configuration, and double-periodic lattices. We find that the excess Josephson current is resonantly enhanced when the Josephson frequency matches the frequency of the plasma mode at the wave vector selected by the lattice structure. The regular lattices exhibit several kinds of instabilities. We find stability regions of the moving lattice in the plane lattice structure - Josephson frequency. A specific lattice structure at given velocity is selected uniquely by boundary conditions, which are determined by the reflection properties of electromagnetic waves generated by the moving lattice. With increase of velocity the moving configuration experiences several qualitative transformations. At small velocities the regular lattice is stable and the phase shift between neighboring layers smoothly decreases with increase of velocity, starting from π for a static lattice. At the critical velocity the lattice becomes unstable. At even higher velocity a regular lattice is restored again with the phase shift smaller than $\pi/2$. With increase of velocity, the structure evolves towards a rectangular configuration.

I. INTRODUCTION

The intrinsic Josephson effect¹ in strongly anisotropic high-temperature superconductors, such as $\text{Bi}_2\text{Sr}_2\text{CaCu}_2\text{O}_x$ (BSCCO), has been a subject of intense experimental study (see review articles^{2,3}). Stack of low-dissipative junctions formed by atomic layers represents a nonlinear system with unique dynamic properties. In particular, this system possesses a rich spectrum of the electromagnetic plasma waves. These waves can be excited via the Josephson effect, which makes these materials convenient voltage-to-frequency converters and gives strong potential for practical applications.

A magnetic field applied along the layers forms the lattice of Josephson vortices. Transport properties of this state are determined by the dynamics of the Josephson vortex lattice. Coherent motion of Josephson vortices in BSCCO has been observed experimentally⁴⁻⁶. The motion of the Josephson lattice generates alternating electric fields and currents which are coupled to electromagnetic plasma waves. One can expect a strong resonance emission when the velocity of the lattice matches the velocity of the plasma wave⁷. In a voltage-biased transport experiment this should be seen as a resonant enhancement of the transport current^{8,9}, while in a current-biased experiment the resonance should be seen as a voltage jump. In conventional long Josephson junctions this effect is known as Eck peak (Eck step)¹⁰ (see also recent article 11 and references therein). However, in layered superconductors this effect has qualitatively new features. The velocity of a plasma wave propagating along the layers strongly depends on the wave vector along the c direction. On the other hand, the traveling Josephson lattice is coupled only to the plasma modes with the wave vectors given by the reciprocal wave vectors of the lattice, i.e., *the wave vector of the resonant mode is determined by the structure of the Josephson lattice*¹². In early theoretical work⁷⁻⁹ it was assumed that the moving lattice preserves its static structure (stretched triangular lattice) and the resonant velocity of the lattice is determined by this structure. We will show that the lattice structure experiences a nontrivial evolution with increase of velocity. Moreover, a regular lattice state always becomes unstable at a certain velocity. Therefore, finding conditions for the resonance emission is a nontrivial problem. Recent numerical studies^{13,14} revealed a very rich dynamic evolution of moving Josephson structures, which includes regular as well as chaotic solutions.

In this paper we analyze the dynamics of the Josephson lattice at strong fields, in the regime of strongly overlapping vortices. In this regime Josephson coupling can be treated perturbatively. This strongly facilitates the analytical analysis of the dynamic structures. Major results have been already reported in the Letter 15. A similar approach has been used to calculate resonant current-voltage dependencies in conventional long Josephson junctions in magnetic field.^{10,16,11} This approach also describes Josephson dynamics at arbitrary magnetic field when all junction are driven

into resistive state by transport current. We will focus on the dynamics in the case of large size samples and will not consider resonances related to finite-size effect (Fiske resonances). The classification of Fiske resonant frequencies for layered superconductors in the case of a moving rectangular lattice has been done by Kleiner.¹⁷ The experimental observation of these modes has been reported by Irie *et. al.*¹⁸

The phase dynamics in layered superconductors is described by the coupled sine-Gordon equations.^{19,12,20,21,8,9} Two equivalent approaches have been used to derive these equations. In the first approach^{19,12,20} the layered superconductor is modeled as a multilayered S-I-S-I... system and the parameters of the equations are expressed via the geometrical parameters and the bulk parameters of the superconducting material from which the superconducting layers are prepared. The second approach^{21,8,9}, more natural for atomically layered superconductors, is based on the Lawrence-Doniach model. In this approach the layers are treated as two-dimensional entities from the very beginning. We will use the second approach.

The dynamic phase diagram strongly depends on dissipation mechanisms. Moving Josephson vortices generate both in-plane and out-of-plane electric fields which induce dissipative quasiparticle currents. Usually, only dissipation due to the tunneling of quasiparticles between the layers is taken into account in consideration of the dynamics of the Josephson vortices.^{22,19} However, in high- T_c superconductors the in-plane component of the quasiparticle conductivity σ_{ab} is strongly enhanced in the superconducting state as compared to the normal conductivity due to the reduction of the phase space for scattering. This enhancement was observed in $YBa_2Cu_3O_7$ ²³ and in $BSCCO$ ²⁴. The c -axis component, σ_c , monotonically decreases with temperature in the superconducting state.^{25,26} The anisotropy of dissipation σ_{ab}/σ_c becomes larger than the superconducting anisotropy γ^2 (here γ is the anisotropy of the London penetration depth). This leads to the dominance of the in-plane dissipation in the dynamics of the Josephson lattice in a wide field range.²⁷

Starting from the the coupled sine-Gordon equations, we derive equations for the relative displacements between the moving Josephson planar arrays in the layers (or, equivalently, for the phase shifts between the Josephson oscillations in the different layers). This allows us to reduce the original two-dimensional problem to a one-dimensional one. Dynamic equations reveal two families of steady-state solutions: lattices with constant phase shifts between neighboring layers, starting from zero for a rectangular configurations to π for a triangular configuration, and double-periodic lattices with the average phase shift $\pi/2$. We analyze the stability of the regular lattices and show that they exhibit several kinds of instabilities including the long-wave length shear instability and the short-wave length instability with respect to alternating deformations. A specific lattice structure at given velocity is selected uniquely by boundary conditions. The numerical investigation shows that at small velocities the lattice experiences a smooth evolution of the structure with the phase shift between neighboring layers decreasing from π at zero velocity to smaller values. At a certain velocity the lattice becomes unstable and the system switches into an oscillating or chaotic state. At even higher velocities the steady-state regular lattice is restored again. The phase shift for this rapidly moving lattice is smaller than $\pi/2$ and continues to decrease with increasing velocity, i.e., the structure evolves smoothly towards a rectangular configurations. The current-voltage characteristic is non-monotonic in the region of the instabilities, which means that two different coherent steady-states coexist within a certain current range. Within this current range the system can also be in the phase separated states, in which it is split into two (or more) domains moving with different velocities separated by a phase defect.

The paper is organized as follows. In Section II we derive the coupled dynamic equations for the in-plane fields and phase differences. In Section III we derive the dynamic equations for the relative displacements [phase shifts] between the Josephson planar arrays in layers. In Section IV we study the coherent steady-states [regular lattices] and calculate the excess Josephson currents and Poynting vectors for such states. In Section V we investigate the stability of the steady-states. We consider in detail two important particular cases of instabilities: the long-wave and short-wave instability. We also compute numerically the stability phase diagrams in the plane structure-Josephson frequency. In Section VI we consider boundary conditions for top and bottom boundaries, discuss the mechanism of structure selection by the boundaries, and numerically calculate the evolution of the lattice structure with increase of velocity. Finally, in Section VII we discuss the mechanism of multiple branches in the current-voltage dependence due to the dynamic phase separation: spontaneous splitting of the system into the rapidly and slowly moving regions.

II. DYNAMIC EQUATIONS

The dynamics of the moving Josephson lattice can be described by coupled equations for the phase differences and magnetic field. These equations can be derived from Maxwell's equations expressing fields and currents in terms of the gauge invariant phase difference between the layers $\theta_n = \phi_{n+1} - \phi_n - \frac{2\pi s}{\Phi_0} A_z$ and the in-plane superconducting momentum $p_n = \nabla_x \phi_n - \frac{2\pi}{\Phi_0} A_x$ (see, e.g., Ref. 9). Consider a layered superconductor in a magnetic field applied along the layers (y -direction) with transport current flowing along the c -axis (z -direction). A local magnetic field H_n

between the layers n and $n + 1$ can be expressed as

$$H_n(x) = \frac{\Phi_0}{2\pi s} \left(\frac{\partial \theta_n}{\partial x} - p_{n+1} + p_n \right). \quad (1)$$

The components of electric field can be approximately represented as

$$E_x \approx \frac{\Phi_0}{2\pi c} \frac{\partial p_n}{\partial t}; \quad E_z \approx \frac{\Phi_0}{2\pi c s} \frac{\partial \theta_n}{\partial t}. \quad (2)$$

The components of electric current, j_x and j_z , include the quasiparticle and superconducting contributions

$$j_x = \sigma_{ab} \frac{\Phi_0}{2\pi c} \frac{\partial p_n}{\partial t} + \frac{c\Phi_0}{8\pi^2 \lambda_{ab}^2} p_n, \quad (3)$$

$$j_z = \sigma_c \frac{\Phi_0}{2\pi c s} \frac{\partial \theta_n}{\partial t} + j_J \sin \theta_n. \quad (4)$$

where σ_{ab} and σ_c are the components of the quasiparticle conductivity, $j_J = \frac{c\Phi_0}{8\pi^2 s \lambda_c^2}$ is the Josephson current density, and λ_{ab} and λ_c are the components of the London penetration depth. Using the above relations we rewrite the z - and x -component of Maxwell's equation $\frac{4\pi}{c} \mathbf{j} + \frac{\partial \mathbf{D}}{\partial t} = \nabla \times \mathbf{H}$ as

$$\frac{2\sigma_c \Phi_0}{c^2 s} \frac{\partial \theta_n}{\partial t} + \frac{4\pi}{c} j_J \sin \theta_n + \frac{\varepsilon_c \Phi_0}{2\pi c^2 s} \frac{\partial^2 \theta_n}{\partial t^2} = \frac{\partial H_n}{\partial x}, \quad (5)$$

$$\frac{2\sigma_{ab} \Phi_0}{c^2} \frac{\partial p_n}{\partial t} + \frac{\Phi_0}{2\pi \lambda_{ab}^2} p_n = -\frac{H_n - H_{n-1}}{s}. \quad (6)$$

In the second equation we replaced $\partial H/dz$ by discrete derivative $(H_n - H_{n-1})/s$ and neglected the in-plane displacement current (typical frequencies are assumed to be much smaller than the in-plane plasma frequency c/λ_{ab}). Taking discrete derivative of the second equation and using relation (1), we rewrite the second equation in terms of θ_n and H_n ,

$$\left(\frac{4\pi\sigma_{ab}}{c^2} \frac{\partial}{\partial t} + \frac{1}{\lambda_{ab}^2} \right) \left(\frac{\Phi_0}{2\pi s} \frac{\partial \theta_n}{\partial x} - H_n \right) = -\frac{H_{n+1} + H_{n-1} - 2H_n}{s^2}. \quad (7)$$

Equations (5) and (7) describe the dynamics in terms of phases $\theta_n(x, t)$ and field $H_n(x, t)$. They are equivalent to equations derived in Refs. 8,9. In the case of negligible in-plane dissipation ($\sigma_{ab} = 0$) these equations can be reduced to coupled system of equations for the phases θ_n , which were used in Refs. 19,12,20,21. Equations (5) and (7) provide a simplified description of the phase dynamics. In real systems this dynamics can also be influenced by the charging effects²⁸ and the quasiparticle imbalance²⁹. However, at present there is no experimental information, which would allow to describe these effects quantitatively.

To simplify the analysis of dynamic equations (5) and (7), we introduce the reduced coordinate $u = x/\gamma s$, time $\tau = \omega_p t$, and magnetic field $h_n = H_n 2\pi\gamma\lambda^2/\Phi_0$. We also introduce the reduced penetration depth $l = \frac{\lambda_{ab}}{s}$ and the dissipation parameters (reduced conductivities)³⁰ $\nu_c = \frac{4\pi\sigma_c}{\varepsilon_c \omega_p}$, $\nu_{ab} = \frac{4\pi\sigma_{ab}\lambda^2\omega_p}{c^2}$, which are related as $\nu_c/\nu_{ab} = \sigma_c \gamma^2/\sigma_{ab}$. In terms of these variables Eqs. (5) and (7) acquire a much simpler form

$$\frac{\partial^2 \theta_n}{\partial \tau^2} + \nu_c \frac{\partial \theta_n}{\partial \tau} + \sin \theta_n - \frac{\partial h_n}{\partial u} = 0, \quad (8)$$

$$\left(\nabla_n^2 - \frac{1}{l^2} \right) h_n + \frac{\partial \theta_n}{\partial u} + \nu_{ab} \frac{\partial}{\partial \tau} \left(\frac{\partial \theta_n}{\partial u} - \frac{h_n}{l^2} \right) = 0, \quad (9)$$

which we will use in our analysis. Here ∇_n^2 denotes the discrete Laplace operator, $\nabla_n^2 h_n \equiv h_{n+1} + h_{n-1} - 2h_n$.

In certain special cases the quasiparticle conductivity can be directly related with the Josephson current. The most known example of such relation is the Ambegaokar-Baratoff formula for conventional Josephson junctions.³¹ Latyshev *et. al.*²⁶ have found a similar relation for BSCCO at small temperatures, $j_J = \pi \sigma_c \Delta_0/(es)$, with Δ_0 being the maximum gap. This relation was derived assuming d-wave symmetry of the order parameter and coherent interlayer tunneling. Using this relation we obtain a simple estimate for the c -axis dissipation parameter ν_c at small T ,

$$\nu_c \approx \frac{\omega_p}{2\pi \Delta_0}, \text{ at } T \rightarrow 0.$$

Taking parameters, typical for slightly underdoped BSCCO at $T \approx 50\text{K}$: $\gamma = 500$, $\lambda_{ab} = 240 \text{ nm}$, $s = 15 \text{ \AA}$, $\rho_{ab} \equiv \sigma_{ab}^{-1} = 50 \mu\Omega\cdot\text{cm}$, and $\rho_c \equiv \sigma_c^{-1} = 600 \Omega\cdot\text{cm}$, we obtain estimates $\nu_{ab} \approx 0.1$ and $\nu_c \approx 0.002$, which we will use in the numerical computations. As we can see, typically the in-plane dissipation is much stronger than the c-axis dissipation. Models, which take into account only the c-axis dissipation channel, are not suitable for the quantitative comparison with experiments in BSCCO. Meanings, definitions, and practical formulas for the dimensionless parameters are summarized in Table 1.

III. EQUATIONS FOR RELATIVE DISPLACEMENTS [PHASE SHIFTS] BETWEEN THE JOSEPHSON PLANAR ARRAYS.

At high magnetic fields $H > \Phi_0/(5.5\gamma s^2)$ ($h > l^2/5.5$) strongly overlapping Josephson vortices fill all the layers.³² In this regime the Josephson coupling can be treated perturbatively. Without the Josephson coupling (i.e., dropping $\sin\theta_n$ in Eq. (8)) the phases θ_n change in space and time as

$$\theta_n^{(0)}(\tau, u) = \omega_E\tau + k_H u + \phi_n \quad (10)$$

where the frequency ω_E is set by the electric field E_z , $\omega_E = 2\pi c s E_z / (\Phi_0 \omega_p)$ and the smooth function $k_H(u)$ is connected with the local magnetic field as $d(k_H u)/du = h/l^2$. In general, the local field h varies in space due to self-field of the transport current. In the following we consider a situation when the self-field of current is much smaller than the applied field and neglect its contribution to h . In this case $k_H(u)$ can be approximated by a constant, $k_H = h/l^2 \equiv 2\pi H \gamma s^2 / \Phi_0$. Therefore Eq. (10) represents the phase modulation moving with the velocity $v_E = \omega_E/k_H = cE_z/H$. The phase shift ϕ_n characterizes a relative coordinate of the Josephson lattice in the layer n . Change of the phase shift $\delta\phi_n$ corresponds to the displacement of the lattice at distance $\delta\phi_n/k_H$. Without the Josephson interaction the system would be degenerate with respect to the phase shifts ϕ_n . The Josephson coupling eliminates this degeneracy. It either leads to the slow dynamics of the phase shifts ϕ_n or selects a specific steady-state structure. We will derive a closed set of equations governing the dynamics of the phase shifts $\phi_n(\tau)$. This can be done using an expansion with respect to the Josephson currents and averaging out rapidly oscillating degrees of freedom. Since the compression deformations of the lattice have much higher stiffness in comparison with the shear deformations, one can neglect the explicit coordinate dependence of ϕ_n . In the first order with respect to the Josephson current, the phases $\theta_n(\tau, u)$ and field $h_n(\tau, u)$ acquire the oscillating corrections, $\tilde{\theta}_n(\tau, u)$ and $\tilde{h}_n(\tau, u)$, so that they can be represented as

$$\theta_n(\tau, u) = \omega_E\tau + k_H u + \phi_n(\tau) + \tilde{\theta}_n(\tau, u), \quad (11)$$

$$h_n(\tau, u) = h(u) + \tilde{h}_n(\tau, u), \quad (12)$$

with $\langle d\phi_n/d\tau \rangle_n = 0$. Substituting $\theta_n(\tau, u)$ into Eq. (8) and averaging it with respect to u we obtain the current conservation condition

$$\nu_c \frac{d\phi_n}{d\tau} + i_{Jn} = i_J. \quad (13)$$

Here $i_{Jn} = \langle \sin\theta_n \rangle_u$ is the local Josephson current between the layers n and $n+1$ averaged with respect to the in-plane coordinate u and $i_J = \langle \sin\theta_n \rangle \equiv \langle \langle \sin\theta_n \rangle_u \rangle_n$ is the Josephson current averaged over the layer index. The last current obeys the macroscopic equation $\nu_c \omega_E + i_J = \partial h / \partial u$. In the following, we will assume that $d\phi_n/d\tau \ll \omega_E$. To obtain a closed set of equations we have to relate the local currents i_{Jn} with the phase shifts ϕ_m and their time derivatives $d\phi_m/d\tau$. For this we have to find the oscillating phases and field and average $\sin\theta_n$ with respect to the rapid space variations. The total Josephson current $i_{Jn} \equiv i_{Jn}[\phi_m, d\phi_m/d\tau]$ consists of the nondissipative (i'_{Jn}) and dissipative (i''_{Jn}) components

$$i_{Jn} = i'_{Jn} + i''_{Jn}. \quad (14)$$

The nondissipative component i'_{Jn} determines interaction between the phase shifts ϕ_n . To the lowest order with respect to $d\phi_n/d\tau$ it depends only on the instantaneous configurations of the phase shifts ϕ_n , $i'_{Jn} \equiv i'_{Jn}[\phi_m]$. The dissipative component i''_{Jn} gives an additional contribution to the dissipation coming from the Josephson coupling, and it is proportional to $d\phi_n/d\tau$ for slow time variations. The first term is determined by the first order oscillating corrections to the phases $\tilde{\theta}_n(u)$ and fields \tilde{h}_n which can be found from equations

$$-\frac{\partial^2 \tilde{\theta}_n}{\partial \tau^2} - \nu_c \frac{\partial \tilde{\theta}_n}{\partial \tau} + \frac{\partial \tilde{h}_n}{\partial u} = \sin(\omega_E \tau + k_H u + \phi_n), \quad (15a)$$

$$\left(\nabla_n^2 - \frac{1}{l^2}\right) \tilde{h}_n + \frac{\partial \tilde{\theta}_n}{\partial u} + \nu_{ab} \frac{\partial}{\partial \tau} \left(\frac{\partial \tilde{\theta}_n}{\partial u} - \frac{\tilde{h}_n}{l^2}\right) = 0. \quad (15b)$$

The Josephson term in the first equation acts like a source generating the electromagnetic wave with the frequency ω_E and in-plane wave vector k_H . To obtain solution of this equation we introduce the phase and field response functions, $G(n, m) \equiv G(n, m; k, \omega)$ and $H(n, m) \equiv H(n, m; k, \omega)$, defined as solutions of equations

$$(\omega^2 - i\nu_c \omega) G(n, m) + ikH(n, m) = \delta_{n,m}, \quad (16a)$$

$$ik(1 + i\nu_{ab}\omega) G(n, m) + \left(\nabla_n^2 - \frac{1 + i\nu_{ab}\omega}{l^2}\right) H(n, m) = 0. \quad (16b)$$

These complex functions give the oscillating phase and field in the m -th layer generated by the oscillating current in the n -th layer. For bulk response both functions depend only on the difference $n - m$ and the solution of Eqs. (16a,b) can be obtained by Fourier transformation. For the function $G(n - m)$ this gives

$$G(n - m; k, \omega) = \int \frac{dq}{2\pi} \exp(iq(n - m)) \mathcal{G}(q, k, \omega), \quad (17)$$

$$\mathcal{G}(q, k, \omega) = \left(\omega^2 - i\nu_c \omega - \frac{k^2(1 + i\nu_{ab}\omega)}{2(1 - \cos q) + (1 + i\nu_{ab}\omega)/l^2}\right)^{-1}.$$

This function will play a very important role in the following derivations. In general, the parameters ν_c and ν_{ab} in the last formula may depend on frequency due to the frequency dependence of the quasiparticle conductivities. The pole of the function $\mathcal{G}(q, k, \omega)$ gives the spectrum of the plasma waves and their damping. The spatial dependence of the function $G(n - m; k, \omega)$ is determined by the complex wave vector $q_+ \equiv q_+(\omega, k)$, which describes propagation and decay of the plasma wave along the z axis for the given frequency ω and in-plane wave vector k ,

$$G(n; k, \omega) = \frac{\delta_n}{\omega^2 - i\nu_c \omega} - \frac{k^2(1 + i\nu_{ab}\omega) \exp(iq_+|n|)}{(\omega^2 - i\nu_c \omega)^2 2i \sin q_+}, \quad (18)$$

$$\cos q_+ = 1 - \frac{k^2(1 + i\nu_{ab}\omega)}{2(\omega^2 - i\nu_c \omega)} + \frac{1 + i\nu_{ab}\omega}{2l^2}, \text{ with } \text{Im}[q_+] > 0. \quad (19)$$

Now we can represent the solution of Eqs. (15a,b) for the oscillating phase $\tilde{\theta}_n(\tau, u)$ in the form

$$\tilde{\theta}_n(\tau, u) = \text{Im} \left[\sum_m G(n - m; k_H, \omega_E) \exp(i\omega_E \tau + ik_H u + i\phi_m) \right], \quad (20)$$

and calculate the nondissipative current $i'_{Jn}[\phi_n]$ in Eq. (13):

$$\begin{aligned} i'_{Jn}[\phi_n] &= \langle \tilde{\theta}_n(\tau, u) \cos(\omega_E \tau + k_H u + \phi_n) \rangle_u \\ &= \frac{1}{2} \sum_m \text{Im} [G(n - m; \omega_E) \exp(-i(\phi_n - \phi_m))]. \end{aligned} \quad (21)$$

This term determines the nonlocal dynamic interactions between different ϕ_n . As follows from Eq. (18), the range of interaction is given by the length $L_s(k_H, \omega_E) = (\text{Im}[q_+(k_H, \omega_E)])^{-1}$. At $\omega_E = 0$ interactions extend only over the nearest neighbors. The range of interactions increases with increase of lattice velocity. When the velocity exceeds the minimum velocity of propagating electromagnetic wave, the range of interactions is limited only by dissipation.

To describe the slow phase dynamics, one has to find also the dissipative component of the Josephson current $i''_{Jn}[\phi_n, d\phi_n/d\tau]$. It is determined by the oscillating contributions to the phases and fields of the order of $\tilde{\theta}_n d\phi_n/d\tau$ which we notate as θ_{dn} and h_{dn} . Representing $\tilde{\theta}_n$ and \tilde{h}_n in the complex form $\tilde{\theta}_n, \tilde{h}_n \propto \exp(i\omega_E \tau + ik_H u)$, we obtain the following equations for θ_{dn} and h_{dn}

$$\begin{aligned} (\omega_E^2 - i\nu_c \omega_E) \theta_{dn} + ik_H h_{dn} &= \frac{\partial \phi_n}{\partial \tau} (-2\omega_E + i\nu_c) \tilde{\theta}_n, \\ \nabla_n^2 h_{dn} - \frac{1 + i\nu_{ab}\omega_E}{l^2} h_{dn} + ik_H (1 + i\nu_{ab}\omega_E) \theta_{dn} &= \frac{\partial \phi_n}{\partial \tau} \left(i\nu_{ab} \frac{\tilde{h}_n}{l^2} + \nu_{ab} k_H \tilde{\theta}_n \right). \end{aligned}$$

Solution for θ_{dn} can be represented as

$$\theta_{dn} = \sum_{n_1, m} \text{Im} \left[F(n - n_1, n_1 - m) \frac{\partial \phi_{n_1}}{\partial \tau} \exp(i\omega_E \tau + ik_H u + i\phi_m) \right],$$

where the kernel $F(n, m) \equiv F(n, m; k_H, \omega_E)$ is defined by relations

$$F(n, n_1) = \int \frac{dq dq_1}{(2\pi)^2} \mathcal{F}(q, q_1) \exp(iqn + iq_1 n_1), \quad (22)$$

$$\mathcal{F}(q, q_1) = \left(-2\omega_E + i\nu_c + \frac{ik_H^2 \nu_{ab}}{2(1 - \cos q) + \frac{1+i\nu_{ab}\omega_E}{l^2}} \frac{2(1 - \cos q_1)}{2(1 - \cos q_1) + \frac{1+i\nu_{ab}\omega_E}{l^2}} \right) \mathcal{G}(q) \mathcal{G}(q_1), \quad (23)$$

with $\mathcal{G}(q) \equiv \mathcal{G}(q, k, \omega)$ being the response function defined by Eq. (17). Using this solution we can now obtain the term $i''_{Jn}[\phi_n, d\phi_n/d\tau]$

$$\begin{aligned} i''_{Jn}[\phi_n, d\phi_n/d\tau] &= \langle \theta_{dn}(\tau, u) \cos(\omega_E \tau + k_H u + \phi_n) \rangle_u \\ &= \frac{1}{2} \sum_{n_1, m} \text{Im} \left[F(n - n_1, n_1 - m) \frac{\partial \phi_{n_1}}{\partial \tau} \exp(i(\phi_m - \phi_n)) \right]. \end{aligned} \quad (24)$$

Substituting averages (21) and (24) into Eq. (13) we finally obtain:

$$\sum_m \nu_{n-m}[\phi_j] \frac{d\phi_m}{d\tau} + \frac{1}{2} \sum_m \text{Im} [G(n - m) \exp(i(\phi_m - \phi_n))] = i_J, \quad (25)$$

where the nonlocal viscosity matrix $\nu_{n-m}[\phi_j]$ depends on the instantaneous phase configuration and is given by

$$\nu_{n-m}[\phi_j] = \nu_c \delta_{n-m} + \frac{1}{2} \sum_j \text{Im} [F(n - m, m - j) \exp(i(\phi_j - \phi_n))] \quad (26)$$

and the average Josephson current i_J is given by

$$i_J = \frac{1}{2} \sum_m \langle \text{Im} [G(n - m) \exp(-i(\phi_n - \phi_m))] \rangle_{n, \tau}. \quad (27)$$

These equations describe the slow dynamics of the phase shifts ϕ_n imposed by the Josephson coupling. Our further analysis is based on these equations. Eqs. (25) and (26) are valid far away from the top and bottom. This means that in a stack consisting of a finite number of junctions N , these equations have a region of validity only if N is much larger than the decay length of electromagnetic wave along the c direction $L_s(k_H, \omega_E) = (\text{Im}[q_+(k_H, \omega_E)])^{-1}$, which determines the range of the phase interactions. In Fig. 2 we plot the dependence of the decay length L_s on the Josephson frequency ω_E for several values of k_H using parameters $\nu_{ab} = 0.1$ and $\nu_c = 0.002$. For small fields one can see a significant increase of L_s when ω_E exceeds the minimum frequency, $\omega_{\min} = k_H/2$, for the electromagnetic wave with the in-plane wave vector k_H . Nevertheless for stacks, containing 50-100 junctions, the bulk behavior is expected in a wide range of fields. The same stack can be either in the bulk regime or in the finite-size regime depending on electric and magnetic fields.

IV. COHERENT STEADY-STATES AND RESONANT I-V DEPENDENCIES

In steady-states we have $d\phi_n/d\tau = 0$ and the static phase shifts ϕ_n far away from the boundaries obey equations

$$\frac{1}{2} \sum_m \text{Im} [G(n - m) \exp(-i(\phi_n - \phi_m))] = i_J. \quad (28)$$

These equations have a trivial solution

$$\phi_n = \kappa n, \quad (29)$$

corresponding to a regular lattice. In this solution the planar arrays in the neighboring layers are shifted by the fraction $\kappa/2\pi$ of the lattice constant (see Fig. 1a). In particular, $\kappa = 0$ corresponds to a rectangular lattice, and $\kappa = \pi$ corresponds to a triangular lattice giving a ground state at $\omega_E = 0$. The oscillating phase (20), $\tilde{\theta}_n \equiv \tilde{\theta}_n(\kappa, k_H, \omega_E)$, and the average Josephson current (27), $i_J \equiv i_J(\kappa, k_H, \omega_E)$, for the moving regular lattice are given by

$$\tilde{\theta}_n = \text{Im} [\mathcal{G}(\kappa, k_H, \omega_E) \exp i(\omega_E \tau + k_H u + \kappa n)], \quad (30)$$

$$i_J = \frac{1}{2} \text{Im} [\mathcal{G}(\kappa, k_H, \omega_E)]. \quad (31)$$

In the case of relatively weak in-plane dissipation, $\nu_{ab}\omega_E \ll 2l^2(1 - \cos \kappa) + 1$, the Josephson current acquires a simple resonant dependence on the Josephson frequency ω_E (electric field)

$$i_J = \frac{1}{2} \frac{\omega_E \nu(\kappa)}{(\omega_E^2 - \omega_p^2(\kappa))^2 + (\omega_E \nu(\kappa))^2} \quad (32)$$

where

$$\omega_p(\kappa) = \frac{k_H}{\sqrt{2(1 - \cos \kappa) + 1/l^2}}$$

is the plasma frequency at the wave vector κ and

$$\nu(\kappa) \equiv \nu_c + \frac{2(1 - \cos \kappa) k_H^2 \nu_{ab}}{(2(1 - \cos \kappa) + \frac{1}{l^2})^2}.$$

is the κ -dependent dissipation parameter. When the Josephson frequency ω_E matches the frequency of the corresponding plasma wave $\omega_p(\kappa)$, a resonance enhancement of the current is expected. Using this result we can represent the current-voltage characteristic as

$$j_z = \sigma_c E_z \left(1 + \frac{1}{2} \frac{E_p^4 \nu(\kappa) / \nu_c}{(E_z^2 - E_r^2(\kappa))^2 + (E_p E_z \nu(\kappa))^2} \right), \quad (33)$$

where

$$E_r(\kappa) = \frac{Hs/\lambda_{ab}}{\sqrt{\varepsilon_c} \sqrt{2(1 - \cos \kappa) + s^2/\lambda_{ab}^2}}$$

is the resonance electric field and $E_p \equiv \Phi_0 \omega_p / (2\pi cs)$ is the electric field at which the Josephson frequency matches the plasma frequency. This expression is similar to Eck peak for a single junction.¹⁰ However, in contrast to a single junction, both the resonance frequency and the dissipation parameter depend on lattice structure. An important scale of the electric field is set by the minimum frequency of the propagating plasma modes, corresponding to the triangular lattice

$$E_{\min} \equiv E_r(\pi) \approx \frac{Hs}{4\lambda_{ab}\sqrt{\varepsilon_c}}.$$

For BSCCO ($\lambda_{ab} = 220$ nm, and $s = 15$ Å, $\varepsilon_c = 11$) this field typically corresponds to the voltage drop of ≈ 0.48 mV per junction at $H = 1$ tesla. At fixed electric field the triangular configuration ($\kappa = \pi$) gives the highest dissipation and the highest current, while the rectangular configuration ($\kappa = 0$) gives the lowest dissipation and the smallest current. There are two reasons for this property. Firstly, the triangular configuration has the smallest resonance frequency $\omega_p(\pi) \approx k_H/2$ and the rectangular configuration has the largest resonance frequency $\omega_p(0) = lk_H$ exceeding $\omega_p(\pi)$ by the factor $2l = 2\lambda_{ab}/s \approx 300$. Secondly, the in-plane contribution to dissipation is completely absent for the rectangular lattice and it is maximum for the triangular lattice. Eq. (33) can be used for the direct comparison with experiment only at small electric fields, where the structure is close to triangular one. At higher electric fields the lattice structure (parameter κ) changes with the electric field. This evolution of the lattice structure is determined by the boundary conditions and will be considered below.

The motion of the regular Josephson lattice generates a traveling electromagnetic wave inside the superconductor. The energy flux in this wave is given by the Poynting vector

$$\mathbf{P} = \frac{c}{4\pi} [\tilde{\mathbf{E}} \times \tilde{\mathbf{H}}]$$

where $\tilde{\mathbf{E}}$ and $\tilde{\mathbf{H}}$ are the oscillating components of the electric and magnetic fields. Using expression for the y component of the magnetic field, \tilde{H}_y , and for the components of the electric field, \tilde{E}_x and \tilde{E}_z ,

$$\begin{aligned}\tilde{H}_y &= \frac{\Phi_0}{2\pi\gamma\lambda^2} \text{Im} \left[\frac{ik_H(1 + i\nu_{ab}\omega_E)\mathcal{G}(\kappa, k_H, \omega_E)}{2(1 - \cos\kappa) + (1 + i\nu_{ab}\omega_E)/l^2} \exp(i(k_Hx + \kappa n + \omega_E t)) \right], \\ \tilde{E}_x &= \frac{\Phi_0\omega_p}{2\pi cs\gamma} \text{Im} \left[\frac{k_H\omega_E(1 - \exp(-i\kappa))\mathcal{G}(\kappa, k_H, \omega_E)}{2(1 - \cos\kappa) + (1 + i\nu_{ab}\omega_E)/l^2} \exp(i(k_Hx + \kappa n + \omega_E t)) \right], \\ \tilde{E}_z &= \frac{\Phi_0\omega_p}{2\pi cs} \text{Im} [i\omega_E\mathcal{G}(\kappa, k_H, \omega_E) \exp(i(k_Hx + \kappa n + \omega_E t))],\end{aligned}$$

we obtain the components of the Poynting vector,

$$P_x = P_{ab} \frac{\omega_E k_H (2(1 - \cos\kappa) + (1 - \nu_{ab}^2 \omega_E^2)/l^2)}{|2(1 - \cos\kappa) + (1 + i\nu_{ab}\omega_E)/l^2|^2} |\mathcal{G}(\kappa, k_H, \omega_E)|^2, \quad (34)$$

$$P_z = P_c \frac{\omega_E k_H^2 (\sin\kappa - \nu_{ab}\omega_E(1 - \cos\kappa))}{|2(1 - \cos\kappa) + (1 + i\nu_{ab}\omega_E)/l^2|^2} |\mathcal{G}(\kappa, k_H, \omega_E)|^2, \quad (35)$$

with

$$P_{ab} = \frac{\Phi_0^2 \omega_p}{32\pi^3 \lambda^2 s \gamma}, \quad P_c = P_{ab}/\gamma. \quad (36)$$

For the typical parameters of BSCCO ($\lambda = 200\text{nm}$, $\gamma = 500$, $\omega_p/2\pi = 150\text{ GHz}$), the scale of the in-plane Poynting vector can be estimated as, $P_{ab} \approx 125\text{ W/cm}^2$.

At small electric fields the lattice is triangular and Eq. (33) gives the linear flux-flow conductivity. We represent it in the form convenient for comparison with experiment

$$\sigma_c^{ff} \approx \sigma_c \left(1 + \frac{1}{2} \left(\frac{\Phi_0}{\pi H \gamma s^2} \right)^4 \right) + \frac{\sigma_{ab}}{2\gamma^2} \left(\frac{\Phi_0}{\pi H \gamma s^2} \right)^2 \quad (37)$$

We neglected here small terms $\sim 1/l^2$. This result, valid at $H > \Phi_0/\pi\gamma s^2$, was first derived in Ref. 8. An important feature of this dependence is the H^{-2} term coming from the in-plane dissipation. In high- T_c superconductors suppression of scattering leads to a strong enhancement of the in-plane quasiparticle conductivity, which is seen as a pronounced peak in the temperature dependence of σ_{ab} ^{23,24}. On the other hand, σ_c monotonically decreases when the temperature goes down. The inequality $\sigma_{ab} \gg \sigma_c \gamma^2$ holds almost everywhere in the superconducting state. In this case Eq. (37) predicts the quadratic dependence of the flux flow resistivity $\rho_c^{ff} \propto H^2$ in a wide field range $\Phi_0/\pi\gamma s^2 < H < \sqrt{\sigma_{ab}/\sigma_c \gamma^2} \Phi_0/\pi\gamma s^2$.²⁷ In contrast, for the case of dominating c-axis dissipation, the flux-flow conductivity at high fields coincides with the c-axis quasiparticle conductivity and it is field independent. Eq. (37) describes very well the field dependence of the flux-flow resistivity in BSCCO.³³

Another important case, which is realized at high currents, is the rectangular lattice with $\kappa = 0$. In this limit Eq. (33) significantly simplifies

$$j_z = \sigma_c E_z \left(1 + \frac{1}{2} \frac{E_p^4}{(E_z^2 - E_r^2(0))^2 + (E_p E_z \nu_c)^2} \right), \quad (38)$$

where $E_r(0) = H/\sqrt{\varepsilon_c}$ is the largest resonance field. Note that in this limit the in-plane dissipation does not influence any more the lattice dynamics. A pronounced resonant feature at $E_z = E_r(0)$ can be observed only for the case of very small c-axis dissipation. The peak amplitude is comparable with the quasiparticle current $\sigma_c E_z$ if

$$H \lesssim \Phi_0/(2\pi\nu_c\lambda_c s).$$

For typical BSCCO parameters this corresponds to fields $\lesssim 1\text{ T}$. Another obvious condition for observation of the resonance is that the voltage drop between the neighboring layers at the resonance field $sE_r(0)$ must be smaller than the gap voltage Δ_0/e , which gives

$$H < H_\Delta = \frac{\Delta_0 \sqrt{\varepsilon_c}}{es}$$

Using $\Delta_0 = 25\text{mV}$ and $\varepsilon_c = 12$ we obtain $H_\Delta \approx 2\text{kG}$.

In addition to the periodic lattices, Eq. (28) allows for the double-periodic solutions of the form

$$\phi_n = \frac{\pi}{2}n + u(-1)^n$$

This can be shown by the direct substitution of this expression into Eq. (28) using the following identities

$$\begin{aligned} \exp(-iu((-1)^n - (-1)^m)) &\equiv 1 + \frac{(1 - (-1)^{n-m})}{2}(\exp(-i(-1)^n 2u) - 1) \\ \sum_m G(m) \exp\left(-i\frac{\pi}{2}m\right) &\equiv \sum_m G(m) \exp\left(i\frac{\pi}{2}m\right) \end{aligned}$$

Such double-periodic lattice is sketched in Fig. 1b. The current i_J for these states does not depend on the modulation parameter u , $i_J(k_H, \omega_E) = \frac{1}{2} \text{Im} [\mathcal{G}(\frac{\pi}{2}, k_H, \omega_E)]$.

V. STABILITY OF COHERENT STEADY-STATES

A. Equations for small deviations from regular lattice and stability criterion

To investigate stability of the moving regular lattice we consider a solution of the form $\phi_n(\tau) = \kappa n + u_n(\tau)$ and obtain equations for the small deformations $u_n(\tau) \ll 1$

$$\begin{aligned} \nu_c \frac{\partial u_n}{\partial \tau} + \frac{1}{2} \sum_{n_1} \text{Im} [F(n - n_1, \kappa) \exp(i\kappa(n_1 - n))] \frac{\partial u_{n_1}}{\partial \tau} \\ + \frac{1}{2} \sum_m \text{Re} [G(n - m; \omega_E) \exp(i\kappa(m - n))] (u_m - u_n) = 0. \end{aligned} \quad (39)$$

Looking for solutions in the form of plane waves

$$u_n = \text{Re}[u_q \exp(\alpha(q)\tau + iqn)],$$

we obtain for the eigenvalue $\alpha(q) \equiv \alpha(q, \kappa, k_H, \omega_E)$

$$\alpha(q) = -\frac{1}{4} \frac{\mathcal{G}(\kappa + q) + \mathcal{G}^*(\kappa - q) - 2 \text{Re} [\mathcal{G}(\kappa)]}{\nu_c + \frac{1}{4i} [\mathcal{F}(\kappa + q, \kappa) - \mathcal{F}^*(-\kappa + q, \kappa)]}. \quad (40)$$

where the functions $\mathcal{G}(q)$ and $\mathcal{F}(q, q_1)$ are given by Eqs. (17) and (23). The lattice is stable if there is no exponentially growing solution in the whole q -interval $0 < q < \pi$, i.e.,

$$\text{Re}[\alpha(q)] < 0, \text{ for } 0 < q < \pi.$$

The instability is characterized by the wave vector q_i , at which $\text{Re}[\alpha(q)]$ becomes positive for the first time. We consider in detail the two important special cases: the long-wave instability at $q_i = 0$ and the instability with respect to alternating deformations at $q_i = \pi$.

According to the generally accepted classification (see, e. g., Ref. 34), one can distinguish two kinds of instability: an absolute instability, for which initial perturbation exponentially grows at any point and a convective instability, for which growing perturbation is drifted away so that it decays with time at fixed point.

B. Long-wave length stability

Formally, the condition of the long-wave stability can be obtained from Eq. (40) at $q \rightarrow 0$. However, for better understanding of the instability mechanism, we will obtain it directly from the equation of motion for the elastic deformation of the lattice (39). To derive this equation, we add to the solution (29) slowly changing in space and

time function $u(\tau, n)$, $\phi_n = \kappa n + u(\tau, n)$, and replace the discrete index n by a continuous variable z . Substituting this expression into Eq. (25), expanding it with respect to $u(\tau, z)$, and performing a gradient expansion, we obtain equation for the elastic deformation $u(\tau, z)$:

$$\nu \frac{\partial u}{\partial \tau} + \zeta \frac{\partial^2 u}{\partial z \partial \tau} + a_1 \frac{\partial u}{\partial z} + a_2 \frac{\partial^2 u}{\partial z^2} + \dots = 0 \quad (41)$$

with

$$a_1 \equiv a_1(\kappa, k_H, \omega_E) = \frac{1}{2} \text{Im} \left[\frac{\partial \mathcal{G}(\kappa, k_H, \omega_E)}{\partial \kappa} \right], \quad (42a)$$

$$a_2 \equiv a_2(\kappa, k_H, \omega_E) = -\frac{1}{4} \text{Re} \left[\frac{\partial^2 \mathcal{G}(\kappa, k_H, \omega_E)}{\partial \kappa^2} \right], \quad (42b)$$

$$\nu \equiv \nu(\kappa, k_H, \omega_E) = \nu_c + \frac{1}{2} \text{Im} \left[\frac{\partial \mathcal{G}(\kappa, k_H, \omega_E)}{\partial \omega_E} \right] \equiv \frac{\partial i(\kappa, k_H, \omega_E)}{\partial \omega_E}, \quad (42c)$$

$$\zeta \equiv \zeta(\kappa, k_H, \omega_E) = -\frac{1}{2} \text{Re} \left[\frac{\partial \mathcal{F}(\kappa + q, \kappa, k_H, \omega_E)}{\partial q} \right]_{q=0}. \quad (42d)$$

In the derivation of the formula for ν (42c) we used the relation $\mathcal{F}(\kappa, \kappa, k, \omega) \equiv \partial \mathcal{G}(\kappa, k, \omega) / \partial \omega$. Note that the coefficients a_1 and ζ vanish for the symmetric lattices with $\kappa = 0, \pi$. Substituting a solution in the form of a plane wave $u(\tau, n) \propto \exp(\alpha(q)\tau + iqn)$ into Eq. (41) we obtain for small q

$$\alpha(q) \approx \frac{1}{\nu} (-ia_1 q + (a_2 - a_1 \zeta / \nu) q^2). \quad (43)$$

This gives the stability condition $\text{Re}[\alpha(q)] < 0$

$$a_2 - a_1 \zeta / \nu < 0; \quad \nu > 0. \quad (44)$$

The first of these conditions means a positive shear stiffness, while the second condition is equivalent to the condition of the monotonic I-V dependence at fixed κ , $\partial i / \partial \omega_E > 0$. On the other hand, formally, the lattice is also stable when *both* inequalities are opposite

$$a_2 - a_1 \zeta / \nu > 0; \quad \nu < 0 \quad (45)$$

The case $a_1 \neq 0$ corresponds to a convective instability. This means that only for symmetric lattices the long-wave instability is an absolute instability. Below we consider several important special cases of the long-range instability.

For the important particular case of the triangular lattice one can find a simple analytical equation for the lowest instability frequency $\omega_\Delta(k_H)$:

$$\omega_\Delta^2 - \frac{k_H^2}{4} = -\omega_\Delta \left(\nu_c + \frac{k_H^2 \nu_{ab}}{4} \right) \left(\sqrt{1 + \nu_{ab}^2 \omega_\Delta^2} - \nu_{ab} \omega_\Delta \right) \quad (46)$$

and for the current at the instability point

$$j_z = j_J \left(\nu_c \omega_\Delta + \frac{1}{2\omega_\Delta \left(\nu_c + \frac{k_H^2 \nu_{ab}}{4} \right)} \frac{1}{\left(\sqrt{1 + \nu_{ab}^2 \omega_\Delta^2} - \nu_{ab} \omega_\Delta \right)^2 + 1} \right)$$

The triangular lattice is stable at $\omega_E < \omega_\Delta(k_H)$, which means that it always becomes unstable before reaching the resonance frequency $\omega_p(\pi) = k_H/2$. The instability point approaches the resonance with decreasing dissipation. In the limit of high in-plane dissipation $\nu_{ab} \gg 2/k_H$ the instability point ω_Δ approaches the universal dissipation-independent value $\omega_\Delta \rightarrow k_H/2\sqrt{2} = \omega_p(\pi)/\sqrt{2}$

The stability boundary of the rectangular lattice $\omega_\square(k_H)$ is given by

$$\omega_\square^2 - l^2 k_H^2 = -\omega_\square \nu_c \left(\nu_{ab} \omega_\square + \sqrt{1 + \nu_{ab}^2 \omega_\square^2} \right)$$

In contrast to the triangular lattice, the rectangular lattice is stable at $\omega_E > \omega_\square(k_H)$ and remains stable at the resonance $\omega_E = lk_H$.

C. Short-wave length instability

To investigate stability of the lattice with respect to alternating deformations we substitute $\phi_n = \kappa n + u(-1)^n$ into Eq. (25). In the linear approximation with respect to the modulation u , it obeys the following simple equation

$$\nu_\pi \frac{du}{d\tau} + a_\pi u = 0, \quad (47)$$

where

$$a_\pi \equiv a_\pi(\kappa, k_H, \omega_E) = -\frac{1}{2} \text{Re} [\mathcal{G}(\kappa) - \mathcal{G}(\pi - \kappa)] \quad (48)$$

$$\nu_\pi \equiv \nu_\pi(\kappa, k_H, \omega_E) = \nu_c + \frac{1}{2} \text{Im} [\mathcal{F}(\kappa - \pi, \kappa)] \quad (49)$$

are the “ π -stiffness” and “ π -viscosity” constants. The stability condition is given by an inequality

$$a_\pi / \nu_\pi > 0 \quad (50)$$

The “ π -stiffness” constant has a symmetry property $a_\pi(\kappa, k_H, \omega_E) = -a_\pi(\pi - \kappa, k_H, \omega_E)$. In particular, $a_\pi(\pi/2, k_H, \omega_E) = 0$, which means that the line $\kappa = \pi/2$ represents the stability boundary for alternating deformations at all lattice velocities. This means that no stability region can cross the line $\kappa = \pi/2$ and *it is impossible to evolve continuously from the static triangular lattice to the rapidly moving rectangular lattice without intersecting the instability boundary*. At small velocities the lattices with $\kappa < \pi/2$ are stable. Above a certain velocity situation is reversed, the lattices with $\kappa > \pi/2$ become stable. This reversal point is determined by the condition $d \text{Re}[G(\kappa)]/d\kappa = 0$ at $\kappa = \pi/2$. Any stability boundary in the region $0 < \kappa < \pi/2$ due to the sign change of $a_\pi(\kappa)$ has the symmetric counterpart in the region $\pi/2 < \kappa < \pi$.

D. Stability phase diagrams

In general, the lattice can become unstable at an arbitrary wave vector $0 < q < \pi$. To find the stability regions of the moving lattice, we numerically scanned the real part of the decay rate $\alpha(q)$ (40) throughout the $\omega_E - \kappa$ phase diagram and find boundaries at which $\text{Re}[\alpha(q)]$ changes sign at least for one q . The obtained stability phase diagram for the representative parameters $\nu_c = 0.002$, $\nu_{ab} = 0.1$, and $k_H = 8$ is shown in Fig. 3. For these parameters we found three stability regions at not very high lattice velocities (Josephson frequencies): the first low-velocity region is located below the resonance line and at $\pi/2 < \kappa \leq \pi$, the second one is located above the resonance line and at $\pi/2 < \kappa \leq \pi$, and the third high-velocity region is located along the resonance line at high velocities with κ approaching 0 with increase of ω_E . At the boundary of the first region the lattice experiences the long-wave instability for $\kappa > 2.04$. At smaller κ instability occurs at finite wave vector $q = q_i$ and the instability wave vector q_i continuously grows with decrease of κ . We find that this behavior occurs due to the sign change of the quartic term in the q -expansion of $\alpha(q)$ and consider in detail this transition in Appendix A. The instability at a finite q always means that the unstable mode has finite frequency ω_i . Close to the instability point the system is expected to generate oscillations with this frequency.

In the velocity range $k_H \ll \omega_E \ll k_H l$ there is only one stability region bounded by two lines above and below the resonance line $\omega_p(\kappa) \approx k_H / \sqrt{2(1 - \cos \kappa)}$, $\kappa_l(\omega_E) < \kappa < \kappa_u(\omega_E)$, see Fig. 4. Both lines correspond to the long-wave instability. In a wide range of frequencies these lines are described by simple analytical formulae, which we derive in Appendix B:

$$\kappa_l(\omega_E) = \frac{k_H}{\sqrt{6}\omega_E}, \quad \text{at } 1/\nu_{ab} < \omega_E < (k_H l)^{2/3} / (6\nu_{ab})^{1/3} \quad (51)$$

$$\kappa_u(\omega_E) = k_H \sqrt{\frac{3\nu_{ab}}{5\omega_E}}, \quad \text{at } 1/\nu_{ab} < \omega_E < \nu_c^{-1/3} \quad (52)$$

As one can see from Fig. 4, these asymptotics agree very well with the numerically calculated stability boundaries.

Fig. 5 shows the evolution of the stability diagram with increase of magnetic field (parameter k_H , see Table 1). Salient features of this evolution are (i) the stability region above the resonance line shrinks with increase of field and vanishes at $k_H > 10$, (ii) the high velocity region expands to higher κ with increase of field, at $k_H \approx 14$ additional a small stability island appears above the line $\kappa = \pi/2$, and at $k_H \approx 16$ this island merges with the the low velocity stability region. This roughly corresponds to the field $\sqrt{\sigma_{ab}/\sigma_c \gamma^2} \Phi_0 / 2\pi \gamma s^2$.

VI. BOUNDARY CONDITIONS AND DYNAMIC STRUCTURE SELECTION

A. General case of sharp boundary

Stability analysis of the previous Section does not show what structure is actually realized at given velocity. For the static case the structure is selected by the minimum energy condition. Such condition is absent in the dynamic case. In this case a particular structure can be selected by the boundary conditions. Influence of the boundary on the moving structure is in turn determined by the interactions of electromagnetic waves with it.

Consider a semiinfinite stack of junctions with $n = 1, 2 \dots$ separated by a sharp boundary from a medium with arbitrary electromagnetic properties. We will obtain boundary conditions for such system in the case of a steady-state. To derive equations for the phase shifts ϕ_n for such system we have to find solution of the linear equations without Josephson coupling taking into account boundary conditions. For the plasma wave with given frequency ω and wave vector along the layers k the oscillating phases (θ_n) and magnetic fields (\tilde{h}_n) in the junctions can be represented as

$$\tilde{\theta}_n, \tilde{h}_n \propto \exp(-iq_+n) + \mathcal{B} \exp(iq_+n), \text{ at } n \geq 1 \quad (53)$$

where $q_+ \equiv q_+(k, \omega)$ is the complex wave vector given by Eq. (19). Properties of the boundary are completely characterized by the complex amplitude of reflected wave $\mathcal{B} \equiv \mathcal{B}(k, \omega)$, which has to be found by matching the solution (53) with electromagnetic oscillations in the medium at $z < 0$. In the case of weak dissipation at $\omega_E > k_H/2$, the wave number q_+ has only small imaginary part and Eq. (53) describes the usual case of reflection of a propagating wave. On the other hand, at $\omega_E < k_H/2$ the wave number q_+ is an almost pure imaginary number and Eq. (53) describes reflection of a decaying wave, which is rarely considered in standard electrodynamics. Note that, in general, $\mathcal{B}(k, \omega)$ can be a complex number with an arbitrary absolute value. Only in the simplest case of vanishing dissipation and propagating wave ($\text{Im}(q_+) = 0$) the amplitude $\mathcal{B}(k, \omega)$ determines a conventional reflection coefficient, $R(k, \omega) = |\mathcal{B}(k, \omega)|^2$, and has property $|\mathcal{B}(k, \omega)| < 1$. In the continuum limit, $q_+ \ll 1$, $\mathcal{B}(k, \omega)$ is given by Fresnel formula (see, e.g., Ref. 35)

$$\mathcal{B}(k, \omega) = \frac{\varepsilon q_+/s - \varepsilon_{ab}(\omega) q_t}{\varepsilon q_+/s + \varepsilon_{ab}(\omega) q_t} \quad (54)$$

where $\varepsilon_{ab}(\omega) = \varepsilon_{ab0} + \frac{4\pi\sigma_{ab}}{i\omega} - \frac{c^2}{\lambda_{ab}^2\omega^2}$ is the in-plane dielectric constant of the superconductor, ε is the dielectric constant of the medium at $z < 0$, and $q_t = \sqrt{\frac{\varepsilon\omega^2}{c^2} - k^2}$ is the wave vector of the transmitted wave.

To derive equations for the phase shifts valid close to the boundary one has to find the phase response function $G(n, m)$ from Eqs. (16a, b) with appropriate boundary conditions. Due to relation (53) the functions $G(n, m)$ should behave as

$$G(n, m) \propto \exp(-iq_+(n-m)) + \mathcal{B} \exp(iq_+(n+m)), \text{ at } 1 \leq n \leq m.$$

Solution of Eqs. (16a,b) satisfying this condition can be constructed as

$$G(n, m) = G(n-m) + \mathcal{B}G(n+m), \quad (55)$$

where the second term describes the surface contribution and vanishes at $n, m \rightarrow \infty$. Equations for the steady-state phase shifts ϕ_n , valid near the boundary, have the following form

$$\frac{1}{2} \sum_{m=1}^{\infty} \text{Im} [G(n, m) \exp(-i(\phi_n - \phi_m))] = i_J \quad (56)$$

In general, a simple ansatz $\phi_n = \kappa n$ does not satisfy the steady-state equations (56) near the surface. A general solution has the form $\phi_n = \kappa n + u_n$, where u_n is the surface deformation, $u_n \rightarrow 0$ at $n \rightarrow \infty$. Equations for u_n can be represented in the form

$$\frac{1}{2} \sum_{m=1}^{\infty} \text{Im} [G(n, m) \exp(-i\kappa(n-m)) (\exp(-i(u_n - u_m)) - 1)] = i_s(\kappa, n) \quad (57)$$

where

$$i_s(\kappa, n) = i_J - \frac{1}{2} \sum_{m=1}^{\infty} \text{Im} [G(n, m) \exp(-i\kappa(n-m))] \quad (58)$$

is the excess Josephson current near the surface, $i_s(\kappa, n) \rightarrow 0$ at $n \rightarrow \infty$. The system (57) is degenerate because it contains only the differences $u_n - u_m$. As a consequence, the solution for u_n exists only for certain values of κ , i.e., *bulk structure is selected by the boundary conditions*. This mechanism of structure selection is realized in many dynamical systems (for a general review see Ref. 36).

The condition for structure selection can be formulated in the explicit form in the case of small surface deformations $u_n \ll 1$, which is always realized at small velocities. In this case Eqs. (57) are reduced to a linear system

$$\frac{1}{2} \sum_{m=1}^{\infty} \text{Re} [G(n, m) \exp(-i\kappa(n-m))] (u_n - u_m) = i_s(\kappa, n). \quad (59)$$

The system (59) is degenerate and its solution exists only for special values of κ .³⁷ To formulate condition for the existence of the solution one has to find a solution ψ_n of the adjoint homogeneous equation

$$\sum_{m=1}^{\infty} (\text{Re} [G(n, m) \exp(-i\kappa(n-m))] \psi_n - \text{Re} [G(n, m) \exp(i\kappa(n-m))] \psi_m) = 0. \quad (60)$$

Eq. (59) has a nontrivial solution only if its right-hand side is orthogonal to ψ_n , i.e.,

$$\sum_{n=1}^{\infty} \psi_n i_s(\kappa, n) = 0. \quad (61)$$

Eqs. (60) and (61) determine the lattice wave vector κ at small velocities.

For finite system, $n = 1, 2, \dots, N$, with identical boundaries the configuration is typically symmetric with respect to the midpoint $n = N/2$, i.e.,

$$\phi_n = \begin{cases} \kappa n, & \text{at } 1 \ll n < N/2 \\ \kappa(N-n), & \text{at } 1 \ll N-n < N/2 \end{cases}$$

In general, these solutions do not match at $n = N/2$, which means that they should be separated by a strongly perturbed region (shock). Further numerical simulations confirm such structure of steady-states in finite systems.

Large class of boundaries is well described by the ideal reflection $\mathcal{B} = -1$. This includes a boundary with an insulator or free space (see Appendix C). In this case the response function $G(n, m)$ in Eq. (56) acquires the form

$$G(n, m) = G(n-m) - G(n+m). \quad (62)$$

We also calculate in Appendix D the reflection amplitude $\mathcal{B}(k_H, \omega_E)$ for the more complicated but practically interesting case of the boundary between the static and moving Josephson lattices. Below we investigate in detail the evolution of the lattice structure for the ideally reflecting boundary.

B. Lattice structure at small velocities

At small velocities the lattice structure is close to the static triangular configuration and the phase shifts can be represented as

$$\phi_n(\tau) = \pi n + u(\tau, n) \quad (63)$$

with $|u(\tau, n+1) - u(\tau, n)| \ll 1$. Firstly, we find the lattice wave vector at small velocities from Eqs.(58), (60), and (61). At $\omega_E \rightarrow 0$ the function $G(n)$ is real and it is only nonzero at $n = -1, 0, 1$ with

$$G(0) \approx -\frac{1}{k_H^2} \left(2 + \frac{1}{l^2} \right); \quad G(\pm 1) \approx \frac{1}{k_H^2}.$$

In this case the solution ψ_n of Eq. (60) reduces to a constant and the condition (61) yields

$$\sum_{n=1}^{\infty} i_s(\kappa, n) = 0. \quad (64)$$

For the ideally reflecting boundary, in a linear approximation with respect to ω_E and $\chi = \pi - \kappa$, the only nonzero components of $i_s(\kappa, n)$ at $n = 1$ and 2 are:

$$i_s(\kappa, 1) \approx \frac{\chi}{2k_H^2} - \left(\nu_{ab} + \frac{2\nu_c(3 + 1/l^2)}{k_H^2} \right) \frac{\omega_E}{2k_H^2}, \quad i_s(\kappa, 2) \approx -\frac{\nu_c \omega_E}{2k_H^4}.$$

Using these expansions we obtain from (64) the following relation

$$\chi = \left(\nu_{ab} + \frac{7 + 2/l^2}{k_H^2} \nu_c \right) \omega_E. \quad (65)$$

This relation determines the deformation of the lattice at small velocities for the ideally reflecting boundary.

To obtain a general dynamic equation for weak lattice deformations, we substitute expansion (65) into Eq.(25), replace the discrete variable n by a continuous variable z , and perform a gradient expansion with respect to $\partial u / \partial z$. This yields the celebrated Burgers equation for $u(\tau, z)$:

$$\nu \frac{\partial u}{\partial \tau} + a_2 \frac{\partial^2 u}{\partial z^2} + b_2 \left(\frac{\partial u}{\partial z} \right)^2 = \delta i_J$$

with

$$\begin{aligned} a_2 &= -\frac{1}{4} \operatorname{Re} \left[\frac{d^2 G(\kappa; 0)}{d\kappa^2} \right]_{\kappa=\pi} \approx -\frac{1}{2k_H^2}, \\ b_2 &= \frac{1}{4} \operatorname{Im} \left[\frac{d^2 G(\kappa; \omega_E)}{d\kappa^2} \right]_{\kappa=\pi} \approx -\left(\frac{8\nu_c}{k_H^2} + \nu_{ab} \right) \frac{\omega_E}{2k_H^2}, \\ \nu &= \nu_c + \frac{1}{2} \operatorname{Im} \left[\frac{\partial G(\pi, \omega_E)}{\partial \omega_E} \right]_{\omega_E=0} \approx \left(1 + \frac{8}{k_H^4} \right) \nu_c + \frac{2}{k_H^2} \nu_{ab}, \\ \delta i_J &= i_J - \frac{1}{2} \operatorname{Im} [G(\pi, \omega_E)] \approx i_J - \left(\frac{4\nu_c}{k_H^2} + \nu_{ab} \right) \frac{2\omega_E}{k_H^2}, \end{aligned}$$

Consider a steady-state configuration, $\partial u / \partial \tau = 0$. For a finite system with N junctions and identical boundaries the deformation is symmetric with respect to the center $z = N/2$. The regions of regular lattices, located at $z < N/2$ and $z > N/2$, are separated by the transitional region near the center where the deformation obeys the equation

$$\alpha \frac{d^2 u}{dz^2} + \left(\frac{du}{dz} \right)^2 = \chi^2,$$

with $\alpha = a_2/b_2 \approx \left[\left(\nu_{ab} + \frac{8\nu_c}{k_H^2} \right) \omega_E \right]^{-1}$, $\chi = \pi - \kappa$, and condition $du/dz \rightarrow \pm\chi$ at $z - N/2 \rightarrow \pm\infty$. This equation has the analytical solution (see, e.g., Ref. 38)

$$u = \alpha \ln \left(\cosh \frac{\chi}{\alpha} \left(z - \frac{N}{2} \right) \right).$$

Using the result (65), we obtain that the width of the transition region $L_t = \alpha/\chi$ is given by

$$L_t = \frac{1}{\left(\nu_{ab} + \frac{8\nu_c}{k_H^2} \right) \left(\nu_{ab} + \frac{7\nu_c}{k_H^2} \right) \omega_E^2}.$$

This length diverges at $\omega_E \rightarrow 0$ as ω_E^{-2} . This means that for a finite system there is a typical crossover frequency ω_N , which is determined by the condition $L_t(\omega_N) = N$. At $\omega_E < \omega_N$ the deformation field has a parabolic shape, typical for strained static systems. At $\omega_E > \omega_N$ the system is split into the two homogeneously tilted lattices separated by the shock.

C. Numerical exploration of steady-states and structure evolution

To find steady-state configurations at all velocities we solved Eq. (56) numerically for the case of ideally reflecting boundary using the same representative parameters ($\nu_c = 0.002$, $\nu_{ab} = 0.1$). The evolution of dependencies $\kappa(\omega_E)$ obtained from these solutions for $k_H = 8$ is shown in Fig. 3 together with the stability regions. We found that at small velocities (Josephson frequency ω_E) the lattice structure smoothly evolves with increase of velocity and the lattice wave vector κ decreases from π at zero velocity towards $\pi/2$. The lattice structures in this region are shown in the left columns of Fig. 6. At certain velocity the lattice crosses the instability boundary. This velocity corresponds to the endpoint of the first flux-flow branch. It is close but not identical to the minimum velocity, $\omega_E/k_H = c_{\min}$, of the plasma wave (in reduced units $c_{\min} = 1/2$ and in real units $c_{\min} = cs/(2\lambda_{ab}\sqrt{\varepsilon_c}) \approx 3 \cdot 10^7 \text{cm/sec}$). At higher velocities the periodic lattice with the phase shift smaller than $\pi/2$ is restored. The structure continues to evolve smoothly towards a rectangular configuration with increasing velocity (see right column at Fig. 6).

Fig. 7 shows the evolution of the current-voltage dependence with increase of the magnetic field. At not very high magnetic field ($k_H < 16$) the current-voltage dependencies have two stable branches, corresponding to the moving regular lattices. The low-velocity branch corresponds to the structure close to a triangular lattice. It terminates at the critical velocity. At small magnetic fields one can see a pronounced current enhancement prior the instability point. The high-velocity branch corresponds to the structure close to a rectangular lattice. The resistivity at this branch is close to the c -axis quasiparticle resistivity. In a wide range of magnetic fields, the stable branches are separated by the broad unstable region where a homogeneous regular lattice state can not exist. In this regime there is a broad range of currents, within which two lattice solutions exist.

To characterize intensity of the electromagnetic wave generated by the moving lattice we plot in Fig. 8 the electric field dependencies of the Poynting vector along the layers (34) at different magnetic fields. The z component of the Poynting vector is always smaller than the ab component, and its sign corresponds to the energy flux from the surface to the bulk. One can see that the intensity of the electromagnetic wave rapidly increases with the electric field reaching a maximum at the instability point. This enhancement of the intensity of the traveling wave indicates that the increase of the current near the instability point is caused by the pumping of energy from a dc source into this wave. This maximum becomes smaller at higher magnetic fields. At higher electric fields the wave intensity decreases with field. Note however that one can expect another resonance at very high lattice velocities, where the velocity reaches the *maximum* velocity of electromagnetic wave, $c_{\max} = c/\varepsilon_c$ (see Section IV). We do not consider this resonance here.

To clarify the role of specific boundary on the forming the lattice structure and the current-voltage dependence, we also made several calculations for the more realistic case of the boundary with the static lattice. The amplitude of the reflected electromagnetic wave $\mathcal{B}(k, \omega)$ for this case is calculated in Appendix D. Fig. 9 shows comparison of the structure evolution and the I-V dependence for the representative parameters $\nu_c = 0.002$, $\nu_{ab} = 0.1$, and $k_H = 6$ with the case of the ideally reflecting boundary. Both cases show an overall similar behavior. The only qualitative difference exists at very small ω_E , where the frequency falls within the range of the acoustic branch in the oscillation spectrum of the static Josephson lattice, $0 < \omega < \sqrt{2}/k_H$ (see Appendix D). In this range the lattice wave vector exceeds π and the energy flux is directed from the bulk to the surface. However, this anomaly is almost invisible in the I-V dependence. It only becomes noticeable at smaller fields or weaker dissipation. In the case of the boundary with the static lattice the structure is closer to a triangular lattice at the first instability point. As a consequence, it has higher current at this point. This difference decreases at higher fields.

VII. MULTIPLE BRANCHES DUE TO DYNAMIC PHASE SEPARATION

We found that for not very high magnetic fields two stable states moving with different velocities may coexist within a certain range of applied current. The dominating in-plane dissipation strongly facilitates such coexistence, because in this case the lattice velocity is very sensitive to the lattice structure. Within the coexistence region one can expect a family of intermediate states, in which the system is split into the two regions moving with different velocities separated by a phase defect (dynamic phase separation, see Fig. (10)). In a continuous system coexistence of the states moving with different velocity at the fixed average velocity is possible only at one driving force, at which these states are in the dynamic equilibrium. Out of equilibrium the boundary will move and eliminate one of the states. However, for our discrete system the boundary separating different lattices is pinned by the discrete structure, and coexistence is possible in a wide range of driving forces (transport currents).

If the fraction f_s of the system is in the slowly moving state with velocity v_s and the remaining fraction $1 - f_s$ is in the rapidly moving state with velocity v_f than the average velocity v_{av} , which determines the observable electric field, is simply given by

$$v_{av} = f_s v_s + (1 - f_s) v_f$$

To investigate the structure of the boundary region, consider an infinite stack, in which the rapidly moving state occupies the region $n > 0$ and the slowly moving state occupies the region $n < 0$. The condition for coexistence of such states is given by

$$\nu_c \omega_f + i_J(\omega_f, \kappa_f) = \nu_c \omega_s + i_J(\omega_s, \kappa_s)$$

where $\omega_f = k_H v_f$ ($\omega_s = k_H v_s$) is the Josephson frequency for the fast (slow) state. In the zero order approximation with respect to the Josephson coupling the phases are given by

$$\begin{aligned} \theta_n &= \omega_f \tau + k_H u + \kappa_f n + u_n, \text{ at } n > 0 \\ &= \omega_s \tau + k_H u + \kappa_s n + v_n, \text{ at } n \leq 0 \end{aligned}$$

To obtain equations for the boundary deformations u_n and v_n we have to find oscillating phases induced by the Josephson currents. The phases and fields, oscillating with the frequency ω_f , are determined by equations

$$\begin{aligned} \nu_c \frac{\partial \tilde{\theta}_n}{\partial \tau} + \frac{\partial^2 \tilde{\theta}_n}{\partial \tau^2} - \frac{\partial \tilde{h}_n}{\partial u} &= -\Theta(n) \sin(\omega_f \tau + k_H u + \kappa_f n + u_n) \\ \left(\nabla_n^2 - \frac{1}{l^2} \right) \tilde{h}_n + \frac{\partial \tilde{\theta}_n}{\partial u} + \nu_{ab} \frac{\partial}{\partial \tau} \left(\frac{\partial \tilde{\theta}_n}{\partial u} - \frac{\tilde{h}_n}{l^2} \right) &= 0 \end{aligned}$$

where $\Theta(n)$ is the step function. Solution for the oscillating phase is given by

$$\tilde{\theta}_n = \text{Im} \left[\sum_{m=0}^{\infty} G_f(n-m) \exp(i(\omega_f \tau + k_H u + \kappa_f n + u_n)) \right]$$

with $G_f(n-m) \equiv G(n-m; \kappa_f, \omega_f)$. Equation for u_n is obtained from condition $\langle \sin \theta_n \rangle = i_J$,

$$\frac{1}{2} \sum_{m=0}^{\infty} \text{Im}[G_f(n-m) \exp(i(\kappa_f(m-n) + u_m - u_n))] = i_J$$

A similar equation can be derived for the boundary deformations of the slow state v_n . Comparing this equation with Eqs. (55) and (56), one can see that the deformations at the boundary between different moving states coincide with the deformations near the nonreflecting boundary ($\mathcal{B} = 0$).

The phase-separated states give the most natural interpretation of the multiple I-V branches observed by Hecht-fischer *et al.* who studied transport properties of Josephson lattice in BSCCO mesas at high magnetic fields.⁵ Note that these branched should not be mixed with the multiple branches at zero magnetic field, which appear due to the switching of the separate junctions into the resistive state. This interpretation can be verified by measuring the spectrum of the microwave irradiation emitting by the stack. Instead of a single peak located at the Josephson frequency corresponding to the average voltage, the spectrum of irradiation should contain two peaks: at the “slow” frequency ω_s with the weight f_s and at the “fast” frequency ω_f with the weight $1 - f_s$.

VIII. CONCLUSIONS

In summary, we performed a detailed investigation of the Josephson lattice dynamics in layered superconductors at high fields. Our main results can be summarized as follows:

- Interaction between Josephson planar arrays in layers is mediated by excited electromagnetic oscillations. The dynamics of these arrays is described by nonlocal and nonlinear equations.
- For the coherent steady-states, the excess Josephson current and the Poynting vector of the generated electromagnetic wave have resonance dependence on the Josephson frequency (electric field). The resonance frequency is the plasma frequency at the wave vector selected by lattice structure. In the case of the dominating in-plane dissipation, typical for high-temperature superconductors, the damping parameter also strongly depends on the lattice structure.

- We investigated stability of the coherent steady-states and found the two major stability regions in the plane lattice structure-lattice velocity: the low-velocity region and the high-velocity region. Exact topology of the stability phase diagrams depends on dissipation and magnetic field.
- Lattice structure at given velocity is selected by boundary. Boundary conditions are determined by the reflection properties of electromagnetic waves, generated by the moving lattice.
- We investigated structure evolution with increase of the lattice velocity. In a wide range of fields there are two stable branches, the low-velocity branch and the high-velocity branch. At low velocities the lattice structure is close to a triangular lattice. This low-velocity branch terminates due to instability at the critical velocity near the minimum velocity of electromagnetic wave. At high velocities structure of the lattice approaches a rectangular configuration.
- Experimentally observed multiple branches in I-V dependencies are interpreted as the phase separated states, in which system is split into the slowly and rapidly moving regions.

IX. ACKNOWLEDGEMENTS

We thank M. Tachiki, R. Kleiner, M. Machida, N. F. Pedersen, Y. Latyshev, and K. Gray for helpful discussions. This work was supported by the US DOE, Office of Sciences, under contract No. W-31-109-ENG-38. AEK also would like to acknowledge support from the Japan Science and Technology Corporation and to thank the National Research Institute for Metals for hospitality.

Appendix A: Continuous transition from the long-wave instability to the finite-q instability

Numerically investigating stability of steady-state we found that the nature of instability of the first flux flow branch depends on the wave vector κ , at which the lattice becomes unstable. If κ is larger than the critical value κ_t than instability occurs at $q = 0$, i.e., $\partial^2\alpha_1/\partial q^2$ changes sign. At $\kappa < \kappa_t$ the lattice becomes unstable at the finite wave vector q_i , i.e., $\alpha_1(q_i) = 0$ at the instability point. The transition is continuous, q_i smoothly grows with decrease of κ starting from $q_i = 0$ at $\kappa = \kappa_t$ (see Fig. 11). This behavior can be explained as follows. At small q the decay rate $\alpha_1(q)$ can be expanded with respect to q

$$\alpha(q) \approx -a_2q^2 - \frac{1}{2}a_4q^4 - \frac{1}{3}a_6q^6.$$

The coefficients a_{2n} in this expansion depend on κ and ω_E . For stable lattices $a_2 > 0$. The coefficient a_2 becomes negative when the frequency ω_E exceeds the long-wave instability boundary $\omega_2(\kappa)$. Near $\omega_2(\kappa)$ one can use linear expansion for a_2

$$a_2 = a_{20}(\omega_2(\kappa) - \omega_E).$$

Lets also define the frequency $\omega_4(\kappa)$, at which the coefficient a_4 changes sign. Near $\omega_4(\kappa)$ we have

$$a_4 = a_{40}(\omega_4(\kappa) - \omega_E).$$

If $\omega_4(\kappa) > \omega_2(\kappa)$ then the instability occurs at $q = 0$. For the first flux flow branch this is the case for $\kappa > \kappa_t$. Otherwise the lattice become unstable at a finite wave vector q_i . The transition between these regimes takes place at the lattice wave vector κ_t defined by

$$\omega_2(\kappa_t) = \omega_4(\kappa_t),$$

i.e., both a_2 and a_4 vanish at $\kappa = \kappa_t$. Lets consider in detail the behavior in the region where κ only slightly smaller than κ_t and the difference $\omega_2(\kappa_t) - \omega_4(\kappa_t)$ is small. In this region we can use linear expansions for both a_2 and a_4 . We define

$$\begin{aligned} \delta &\equiv \omega_E - \omega_4(\kappa), \\ \delta_2 &= \omega_2(\kappa) - \omega_4(\kappa) = (\omega_2' - \omega_4')(\kappa - \kappa_t) > 0, \end{aligned}$$

and represent $\alpha(q)$ in the form

$$\alpha(q) = -a_{20}(\delta_2 - \delta)q^2 + \frac{1}{2}a_{40}\delta q^4 - \frac{1}{3}a_6q^6.$$

With increase of δ the dependence $\alpha(q)$ becomes nonmonotonic at $(a_{40}\delta)^2 > 4a_{20}a_6(\delta_2 - \delta)$. Extremum values of q are determined by solutions of quadratic with respect to q^2 equation

$$a_6q^4 - a_{40}\delta q^2 + a_{20}(\delta_2 - \delta) = 0 \quad (66)$$

and are given by

$$q_{\pm}^2 = \frac{a_{40}\delta}{2a_6} \pm \sqrt{\left(\frac{a_{40}\delta}{2a_6}\right)^2 - \frac{a_{20}(\delta_2 - \delta)}{a_6}},$$

where q_-^2 gives the minimum of $\alpha(q)$ and q_+^2 gives its maximum. The lattice becomes unstable when $\alpha(q_+) = 0$. This equation together with the extremum condition (66) determines the instability point $\delta = \delta_i$ and the wave vector of the unstable mode q_i

$$\delta_i = \frac{8}{3} \frac{a_6 a_{20}}{a_{40}^2} \left(\sqrt{1 + \frac{3a_{40}^2 \delta_2}{4a_6 a_{20}}} - 1 \right),$$

$$q_i^2 = \frac{2a_{20}}{a_{40}} \left(\sqrt{1 + \frac{3a_{40}^2 \delta_2}{4a_6 a_{20}}} - 1 \right).$$

Close to the transition $\delta_2 \ll a_6 a_{20} / a_{40}^2$ we have

$$\delta_i \approx \delta_2 - \frac{3}{16} \frac{a_{40}^2}{a_6 a_{20}} \delta_2^2,$$

$$q_i^2 \approx \frac{3a_{40}\delta_2}{4a_6}.$$

This means that the wave vector q_i of the unstable mode grows as $q_i \propto \sqrt{\kappa_t - \kappa}$ near the transition. The calculated dependence $q_i(\kappa)$ agrees very well with this predictions (see the lower-left inset in Fig. 11).

Appendix B: Stability boundaries in the intermediate frequency range

In this appendix we consider the stability region in the intermediate velocity range, $k_H \ll \omega_E \ll k_H l$, where it is possible to derive simple analytical expressions for the stability boundaries. There is only one stability region in this frequency range located at $\kappa \ll 1$ and limited by two stability boundaries, $\kappa_l(\omega_E)$ and $\kappa_u(\omega_E)$, located below and above the resonance line. Both boundaries $\kappa_l(\omega_E)$ and $\kappa_u(\omega_E)$ correspond to the long-wave instabilities and we will use general relations from Section V B. Assuming inequalities $1/l^2, \nu_{ab}\omega_E/l^2 \ll \kappa^2 \ll 1, \nu_c\kappa^2 \ll \nu_{ab}$ and introducing scaling variables

$$z = \kappa^2 \omega_E^2 / k_H^2, \quad y = \nu_{ab} \omega_E,$$

we present the coefficients from Eqs. (42a-d) in the form

$$a_1 = -\frac{\kappa}{k_H^2} \operatorname{Im} \left[\frac{(1+iy)}{(z-1-iy)^2} \right], \quad (67a)$$

$$a_2 = -\frac{1}{2k_H^2} \operatorname{Re} \left[\frac{(1+iy)(3z+1+iy)}{(z-1-iy)^3} \right], \quad (67b)$$

$$\nu = \nu_c k_H^3 + \frac{\kappa^2}{2\omega_E k_H} \operatorname{Im} \left[\frac{-2z+iy}{(z-1-iy)^2} \right], \quad (67c)$$

$$\zeta = -\omega_E k_H \kappa^3 \operatorname{Re} \left[\frac{2+iy}{(z-1-iy)^3} \right]. \quad (67d)$$

In general, the stability boundaries are determined by Eq. (44). However, at high enough Josephson frequency term $a_1\zeta/\nu$ can be neglected. We focus here on the regime $y \gg 1$. Consider the lower boundary $\kappa_l(\omega_E)$ first. As can be checked from the result for this boundary the term $a_1\zeta/\nu$ is smaller than a_2 at least by the factor $1/y$. Assuming inequality $y \gg z$ we can approximate a_2 in Eq. (67b) by the first expansion term with respect to $1/y$, $a_2 \approx -\frac{(6z-1)}{2k_H^2 y}$. Therefore the lower stability boundary is simply given by $z = 1/6$, consistent with the assumed condition $y \gg z$. This is equivalent to

$$\kappa_l(\omega_E) = \frac{k_H}{\sqrt{6}\omega_E}. \quad (68)$$

This expression for the lower boundary is valid up to $\omega_E < (k_H l)^{2/3}/(6\nu_{ab})^{1/3}$. It is interesting to note that this boundary does not depend on the dissipation parameters.

Let us consider now the upper boundary $\kappa_u(\omega_E)$. The term $a_1\zeta/\nu$ in Eq. (44) can again be neglected if $\kappa^2 \ll \omega_E^2 k_H^2 \nu_c \nu_{ab}$. In this case the upper boundary is again determined by the equation $a_2 = 0$. At $y \gg 1$ this equation has asymptotic solution in the form $z = \alpha y \gg 1$ and in the main order with respect to $1/y$ the constant α is determined by equation

$$\text{Re} \left[\frac{i(3\alpha + i)}{(\alpha - i)^3} \right] = 0,$$

which gives $\alpha = \sqrt{3/5}$. This corresponds to the stability boundary

$$\kappa_u(\omega_E) = k_H \sqrt{\sqrt{\frac{3}{5}} \frac{\nu_{ab}}{\omega_E}} \quad (69)$$

Substituting this expression into the inequality $\kappa^2 \ll \omega_E^2 k_H^2 \nu_c \nu_{ab}$ (condition to neglect the term $a_1\zeta/\nu$ in Eq. (44)), we see that it is equivalent to the condition $\omega_E \gg \nu_c^{-1/3}$, which gives the lower limit of applicability of Eq. (69).

Appendix C: Boundary with an insulator

Consider a semiinfinite stack of junctions with $n = 1, 2, \dots$ bounded by an insulator at semispace $z < 0$ (e.g., by free space). We assume that the transport current is fed to the stack through the first layer. In this case the oscillating electric and magnetic fields induced by the moving Josephson lattice should match with the electromagnetic oscillations in the insulator.

The oscillating electric and magnetic fields decay into the insulator as

$$\begin{aligned} \mathbf{E}(\mathbf{r}, t) &= \mathbf{E}_0 \exp(ik_H x + qz + i\omega_E t), \\ \mathbf{H}(\mathbf{r}, t) &= \mathbf{H}_0 \exp(ik_H x + qz + i\omega_E t), \end{aligned}$$

where $\mathbf{E}_0 = (E_{x0}, 0, E_{z0})$, $\mathbf{H}_0 = (0, H_0, 0)$, $q = \sqrt{k_H^2 - \varepsilon\omega_E^2/c^2}$, and ε is the dielectric constant of the insulator. Maxwell's equation connects E_{x0} and H_0 as

$$-qH_0 = \frac{i\omega_E \varepsilon}{c} E_{x0}.$$

Continuity of the parallel component of the electric field gives the relation

$$E_{x0} = \frac{\Phi_0 i\omega}{2\pi c} p_1,$$

and Eq. (6) gives

$$\left(\frac{2\sigma_{ab}\Phi_0}{c^2} i\omega_E + \frac{\Phi_0}{2\pi\lambda_{ab}^2} \right) p_1 = -\frac{H_1 - H_0}{s}.$$

From the last three equations we obtain the boundary condition

$$s\sqrt{k_H^2 - \varepsilon\omega_E^2/c^2} H_0 = \frac{\varepsilon(\lambda_{ab}\omega_E/c)^2}{1 + 4\pi\lambda_{ab}^2\sigma_{ab}i\omega_E/c^2} (H_1 - H_0). \quad (70)$$

In general case one has to use the complex dielectric constant ε of the medium at the frequency ω_E and wave vector k_H . In reduced variables this equation can be rewritten as

$$\sqrt{k_H^2 - \frac{\varepsilon}{\varepsilon_c l^2} \omega_E^2} h_0 = \frac{\varepsilon}{\varepsilon_c \gamma} \frac{\omega_E^2}{1 + i\nu_{ab}\omega_E} (h_1 - h_0) \quad (71)$$

From this relation we obtain the amplitude of reflected wave

$$\mathcal{B} = -\frac{\sqrt{k_H^2 - \frac{\varepsilon}{\varepsilon_c l^2} \omega_E^2} + \frac{\varepsilon}{\varepsilon_c \gamma} \frac{\omega_E^2}{1 + i\nu_{ab}\omega_E} (1 - \exp(-iq_+))}{\sqrt{k_H^2 - \frac{\varepsilon}{\varepsilon_c l^2} \omega_E^2} - \frac{\varepsilon}{\varepsilon_c \gamma} \frac{\omega_E^2}{1 + i\nu_{ab}\omega_E} (\exp(iq_+) - 1)} \quad (72)$$

In the case $\varepsilon \sim 1$, $k_H \sim 1/\gamma s$, and $\omega_E \sim \omega_p$ we obtain the estimate $h_0 \sim h_1/\gamma\varepsilon_c \ll h_1$. Therefore the condition (71) with high accuracy may be replaced by the much simpler condition $h_0 = 0$, which corresponds to the ideal reflection case, $\mathcal{B} = -1$,

Appendix D: Reflection amplitude for boundary between moving and static lattice

Small mesas are typically used in experiment to enhance transport current density. In this case the transport current flowing in the bulk part of the sample is not sufficient to drive the Josephson lattice there and the moving Josephson lattice in mesa neighbors with the static lattice in the bulk (see inset in Fig. 12). In this appendix we consider electromagnetic properties of such boundary. We assume that the Josephson lattice is static at $n \leq 0$ and moves with constant velocity at $n > 0$. According to the general recipe outlined in Sec. VI A we have to match electromagnetic oscillations in the neighboring medium neglecting Josephson currents in the region of the moving lattice and to find the amplitude of the reflected wave. We consider reflection of the wave $\theta_n \propto \exp(i(k_H u + \omega\tau - iq_+ n))$ coming from above with q_+ given by Eq. (19). This incident wave excites phase and field oscillations of the static lattice. Such oscillations have been theoretically studied in Ref. 8. At high in-plane field these oscillations are described by approximate equations

$$(\omega^2 - i\nu_c\omega) \theta_n - (2\mathcal{C} \sin^2(k_H u + \pi n) + \cos(k_H u + \pi n)) \theta_n + \frac{\partial h_n}{\partial u} = 0, \quad (73a)$$

$$\left(\nabla_n^2 - \frac{1}{l^2}\right) h_n + \frac{\partial \theta_n}{\partial u} + i\nu_{ab}\omega \left(\frac{\partial \theta_n}{\partial u} - \frac{h_n}{l^2}\right) = 0, \quad (73b)$$

where $\mathcal{C} \equiv \langle \cos \theta_n^{(0)}(u) \rangle \approx \frac{4+1/l^2}{2k_H^2}$ and $\theta_n^{(0)}(u) \approx k_H u + \pi n - \frac{4+1/l^2}{k_H^2} \sin(k_H u + \pi n)$ is the static phase difference. The cosine term in the first equation couples oscillations with the in-plane wave vector k_H to the homogeneous mode (at $k_H \gg 1$ coupling to the higher harmonics can be neglected). Eqs. (73a) and (73b) have two types of solutions for the oscillations with the wave vector k_H , with $\theta_n \propto \cos(k_H u)$ and $\theta_n \propto \sin(k_H u)$, which we refer to as the even and odd modes. The incident wave excites both modes but only the even mode is coupled to the homogeneous oscillations of the lattice. For this mode we look for solution in the form $\theta_n(u) = \left(\tilde{\theta} \cos(k_H u) + (-1)^n \tilde{\theta}\right) \exp(-i\chi_e n)$, $h_n(u) = \tilde{h} \sin(k_H u) \exp(-i\chi_e n)$ and derive equations

$$(\omega^2 - i\nu_c\omega) \tilde{\theta} + k_H \tilde{h} = \bar{\theta}, \quad (74a)$$

$$(\omega^2 - \mathcal{C} - i\nu_c\omega) \bar{\theta} = \frac{\tilde{\theta}}{2}, \quad (74b)$$

$$\left(2(1 - \cos \chi_e) + \frac{1 + i\nu_{ab}\omega}{l^2}\right) \tilde{h} + k_H (1 + i\nu_{ab}\omega) \tilde{\theta} = 0, \quad (74c)$$

which determine the eigenvalue χ_e for the given frequency ω and in-plane wave vector k_H as

$$2(1 - \cos \chi_e) = \frac{(\omega^2 - i\nu_c\omega - \mathcal{C})(1 + i\nu_{ab})k_H^2}{(\omega^2 - i\nu_c\omega)(\omega^2 - i\nu_c\omega - \mathcal{C}) - \frac{1}{2}} - \frac{1 + i\nu_{ab}}{l^2}. \quad (75)$$

Being inverted, this equation gives the frequencies of plasma modes at fixed c-axis wave vector χ and their decay. Note that at $\omega = 0$ we obtain the solution corresponding to a homogeneous shift of the lattice, $\chi = \pi$. For weak dissipation this equation has two other important solutions: (i) $\omega \approx \sqrt{\mathcal{C}} \approx \sqrt{2}/k_H$ and χ_e near zero (the endpoint

of the acoustical branch of the oscillation spectrum) (ii) $\omega \approx k_H/2$ and $\chi_e \approx \pi$ (the frequency of the homogeneous plasma mode).

For the odd mode we look for solution in the form $\tilde{\theta}_n = \tilde{\theta} \sin(k_H u) \exp(-i\chi_o n)$; $\tilde{h}_n = \tilde{h} \cos(k_H u) \exp(-i\chi_o n)$ and derive

$$\begin{aligned} & (\omega_E^2 - i\nu_c \omega - \mathcal{C}) \tilde{\theta}_n - k_H \tilde{h} = 0 \\ & - \left(2(1 - \cos \chi_o) + \frac{1 + i\omega\nu_{ab}}{l^2} \right) \tilde{h} + (1 + i\omega\nu_{ab}) k_H \tilde{\theta} = 0 \end{aligned}$$

which gives

$$2(1 - \cos \chi_o) = (1 + i\omega\nu_{ab}) \left(\frac{k_H^2}{\omega^2 - i\nu_c \omega - \mathcal{C}} - \frac{1}{l^2} \right) \quad (76)$$

Because of $\cos(k_H u)$ modulation in the static lattice region the reflected wave contains a backscattered component, with the wave vector $-k_H$, so that the full solution for the oscillating magnetic field has the form

$$\begin{aligned} h &= \exp(ik_H u - iq_+ n) + \mathcal{B} \exp(ik_H u + iq_+ n) + \mathcal{B}_b \exp(-ik_H u + iq_+ n), \text{ at } n > 0 \\ &= \mathcal{A}_e \cos k_H u \exp(-i\chi_e n) + i\mathcal{A}_o \sin k_H u \exp(-i\chi_o n), \text{ at } n \leq 0 \end{aligned}$$

Introducing the reflection amplitudes in the even and odd channels, $\mathcal{B}_e = \mathcal{B} + \mathcal{B}_b$ and $\mathcal{B}_o = \mathcal{B} - \mathcal{B}_b$, we obtain by matching the solutions at $n = 0, 1$ the following equations

$$\begin{aligned} 1 + \mathcal{B}_e &= \mathcal{A}_e \\ \exp(-iq_+) + \mathcal{B}_e \exp(iq_+) &= \mathcal{A}_e \exp(-i\chi_e) \end{aligned}$$

and similar equations for \mathcal{B}_o and \mathcal{A}_o . These equations can be easily solved giving

$$\begin{aligned} \mathcal{B}_e &= - \frac{\exp(-i\chi_e) - \exp(-iq_+)}{\exp(-i\chi_e) - \exp(iq_+)} \\ \mathcal{A}_e &= - \frac{2i \sin(q_+)}{\exp(-i\chi_e) - \exp(iq_+)} \end{aligned}$$

and similar formulas for \mathcal{B}_o and \mathcal{A}_o . These formulas resemble the well-known Fresnel formulas of classical electrodynamics. The amplitude of the reflected wave $\mathcal{B} = \mathcal{B}(k_H, \omega)$, which determines the surface contribution to the response function in Eq. (55), is given by

$$\mathcal{B} = - \frac{1}{2} \left(\frac{\exp(-i\chi_e) - \exp(-iq_+)}{\exp(-i\chi_e) - \exp(iq_+)} + \frac{\exp(-i\chi_o) - \exp(-iq_+)}{\exp(-i\chi_o) - \exp(iq_+)} \right) \quad (77)$$

Where, again, q_+ , χ_e , and χ_o are given by Eqs. (19), (75), and (76). Plot of the frequency dependence of the amplitude and phase of $\mathcal{B}(k_H, \omega)$, $\mathcal{B}(k_H, \omega) = |\mathcal{B}| \exp(i\phi_{\mathcal{B}})$, is shown in Fig. 12. Typically $|\mathcal{B}|$ is large in the small frequency range $0 < \omega^2 \lesssim \mathcal{C}$, where the incident decaying wave excites the propagating acoustic waves in the static lattice. At $\omega^2 > \mathcal{C}$ $|\mathcal{B}|$ rapidly goes to zero, because both media have identical spectrums of electromagnetic waves at high frequencies. Both the amplitude and phase of $\mathcal{B}(k_H, \omega)$ have anomalies at the typical frequencies $\omega = \sqrt{2}/k_H$ and $\omega = k_H/2$ of the oscillation spectrum of the static lattice. These anomalies become more pronounced at lower dissipation and smaller field.

¹ R. Kleiner, F. Steinmeyer, G. Kunkel, and P. Müller, Phys. Rev. Lett. **68**, 2394 (1992).

² R. Kleiner and P. Müller, Phys. Rev. B **49**, 1327 (1994).

³ A. A. Yurgens, Supercond. Sci. Technol. **13**, R85 (2000).

⁴ J. U. Lee, J. E. Nordman, and G. Hohenwarter, Appl. Phys. Lett., **67**, 1471 (1995); J. U. Lee, P. Guptasarma, D. Hornbaker, A. El-Kortas, D. Hinks, and K. E. Gray Appl. Phys. Lett., **71**, 1412 (1997)

- ⁵ G. Hechtfisher, R. Kleiner, A. V. Ustinov, and P. Müller Phys. Rev. Lett. **79**, 1365 (1997); G. Hechtfisher, R. Kleiner, K. Schlenga, W. Walkenhorst, P. Müller, and H. L. Johnson Phys. Rev. B, **55**, 14638 (1997)
- ⁶ Yu. I. Latyshev, P. Monceau, and V. N. Pavlenko, Physica C, **282-287**, 387 (1997); Physica C, **293**, 174 (1997).
- ⁷ T. Koyama and M. Tachiki, Sol. St. Comm. **96**, 367 (1995)
- ⁸ L. N. Bulaevskii, D. Domínguez, M. P. Maley, A. R. Bishop, and B. I. Ivlev, Phys. Rev. B, **53**, 14 601 (1996)
- ⁹ S. N. Artemenko and S. V. Remizov, JETP Lett., **66**, 853 (1997)
- ¹⁰ R. E. Eck, D. J. Scalapino, and B. N. Taylor, Phys. Rev. Lett. **13**, 15 (1964)
- ¹¹ M. Cirillo, N. Grønbech-Jensen, M. R. Samuelsen, M. Salerno, and G. Verona Rinati, Phys. Rev. B, **58**, 12377 (1998)
- ¹² S. Sakai, A. V. Ustinov, H. Kohlstedt, A. Petraglia, and N. F. Pedersen, Phys. Rev. B **50**, 12 905 (1994)
- ¹³ M. Machida, T. Koyama, A. Tanaka, and M. Tachiki Physica C, **330**, 85 (2000)
- ¹⁴ R. Kleiner, T. Gaber, and G. Hechtfisher Phys. Rev. B **62**, 4086 (2000).
- ¹⁵ A. E. Koshelev and I. S. Aranson, Phys. Rev. Lett. **85**, 3938 (2000).
- ¹⁶ I. O. Kulik, JETP Letters, **2**, 84 (1965).
- ¹⁷ R. Kleiner, Phys. Rev. B, **50**, 6919 (1994).
- ¹⁸ A. Irie, Y. Hirai, and G. Oya, Appl. Phys. Lett. **72**, 2159 (1998).
- ¹⁹ S. Sakai, P. Bodin, and N. F. Pedersen, J. Appl. Phys. B **73**, 2411 (1993)
- ²⁰ R. Kleiner, P. Müller, H. Kohlstedt, N. F. Pedersen, and S. Sakai, Phys. Rev. B, **50**, 3942 (1994).
- ²¹ L. N. Bulaevskii, M. Zamora, D. Baeriswyl, H. Beck, and J. R. Clem, Phys. Rev. B, **50**, 12831 (1994)
- ²² J. R. Clem and M. W. Coffey, Phys. Rev. B, **42**, 6209 (1990)
- ²³ M. C. Nuss, P. M. Mankiewich, M. L. O'Malley, E. H. Westerwick, and Peter B. Littlewood, Phys. Rev. Lett. **66**, 3305 (1991); D. A. Bonn, P. Dosanjh, R. Liang, and W. N. Hardy, Phys. Rev. Lett. **68**, 2390 (1992); A. Hosseini, R. Harris, Saeid Kamal, P. Dosanjh, J. Preston, R. Liang, W. N. Hardy, and D. A. Bonn Phys. Rev. B, **60**, 1349 (1999);
- ²⁴ Shih-Fu Lee, D. C. Morgan, R. J. Ormeno, D. M. Broun, R. A. Doyle, J. R. Waldram, and K. Kadowaki Phys. Rev. Lett. **77**, 735 (1996); H. Kitano, T. Hanaguri, Y. Tsuchiya, K. Iwaya, R. Abiru, and A. Maeda J. Low Temp. Phys. **117**, 1241 (1999); J. Corson, J. Orenstein, S. Oh, J. O'Donnell, and J. N. Eckstein, Phys. Rev. Lett. **85**, 2569 (2000).
- ²⁵ A. Yurgens, D. Winkler, N. V. Zavaritsky, and T. Claeson Phys. Rev. Lett. **79**, 5122 (1997).
- ²⁶ Yu. I. Latyshev, T. Yamashita, L. N. Bulaevskii, M. J. Graf, A. V. Balatsky, and M. P. Maley Phys. Rev. Lett. **82**, 5345 (1999).
- ²⁷ A. E. Koshelev, Phys.Rev. B **62**, R3616 (2000).
- ²⁸ T. Koyama, and M. Tachiki, Phys. Rev. B **54**, 16183 (1996); S. N. Artemenko and A. G. Kobel'kov, Phys. Rev. Lett. **78**, 3551 (1997).
- ²⁹ D. A. Ryndyk, Pis'ma Zh. Eksp. Teor. Fiz., **65**, 755 (1997) [JETP Lett., **65**, 791 (1997)]; Phys. Rev. Lett. **80**, 3376 (1998); Zh. Eksp. Teor. Fiz. **116**, 1798 (1999) (JETP **89**, 975 (1999)).
- ³⁰ Dissipation in Josephson junctions is frequently characterized by McCumber parameter β . It is connected with ν_c as $\beta = \nu_c^{-2}$.
- ³¹ V. Ambegaokar and A. Baratoff, Phys. Rev. Lett., **10**, 486 (1963).
- ³² L. N. Bulaevskii and J. R. Clem, Phys. Rev. B, **44**, 10234 (1991); M. Ichioka, Phys. Rev. B, **51**, 9423 (1995).
- ³³ Yu. I. Latyshev, V. N. Pavlenko, S. -J. Kim, and T. Yamashita, Proceedings of 2nd International Symposium on Intrinsic Josephson Effect, Sendai, Japan, August 22-24, 2000.
- ³⁴ E. M. Lifshits, L. P. Pitaevskii, *Physical Kinetics*. Oxford, New York: Pergamon Press, 1981.
- ³⁵ L. D. Landau, E. M. Lifshits, and L. P. Pitaevskii, *Electrodynamics of continuous media*, Oxford [England]: Butterworth-Heinemann, 1995.
- ³⁶ M. C. Cross and P. C. Hohenberg, Rev. Mod. Phys. **65**, 851 (1993).
- ³⁷ An inhomogeneous linear system $\hat{A}\mathbf{x} = \mathbf{b}$ with a singular matrix \hat{A} , $\det\hat{A} = 0$, has a solution only if its righthand side \mathbf{b} is orthogonal to all nontrivial solutions \mathbf{y} of the homogenous adjoint system, $\hat{A}^\dagger\mathbf{y} = \mathbf{0}$, with $A_{nm}^\dagger = A_{mn}^*$ (see, e.g., V. I. Smirnov, *Linear Algebra and Group Theory*, McGraw-Hill, New York, Toronto, London, 1961).
- ³⁸ Y. Kuramoto, *Chemical Oscillations, Waves, and Turbulence*. Springer Series in Synergetics, Berlin, 1984.

Table 1. Meanings, definitions and practical formulas for the reduced parameters used throughout the paper. In practical formulas $f_p = \omega_p/2\pi$ means plasma frequency, ρ_c and ρ_{ab} are the components of the quasiparticle resistivity

Notation	Meaning	Definition(CGS)	Practical formula (BSCCO)
ω_E	reduced Josephson frequency	$\frac{2\pi c s E_z}{\Phi_0 \omega_p}$	$\frac{(sE_z)[\text{mV}]}{2 \cdot 10^{-3} f_p [\text{GHz}]}$
k_H	wave vector of Josephson lattice	$\frac{2\pi H \gamma s^2}{\Phi_0}$	
ν_c	c-axis dissipation parameter	$\frac{4\pi \sigma_c}{\varepsilon_c \omega_p}$	$\frac{1.8 \cdot 10^3}{\varepsilon_c \rho_c [\Omega \cdot \text{cm}] f_p [\text{GHz}]}$
ν_{ab}	in-plane dissipation parameter	$\frac{4\pi \sigma_{ab} \lambda_{ab}^2 \omega_p}{c^2}$	$\frac{0.79 (\lambda_{ab} [\mu\text{m}])^2 f_p [\text{GHz}]}{\rho_{ab} [\mu\Omega \cdot \text{cm}]}$
l	reduced London penetration depth	λ_{ab}/s	
h	reduced local magnetic field	$\frac{2\pi \gamma \lambda_{ab}^2 H}{\Phi_0}$	

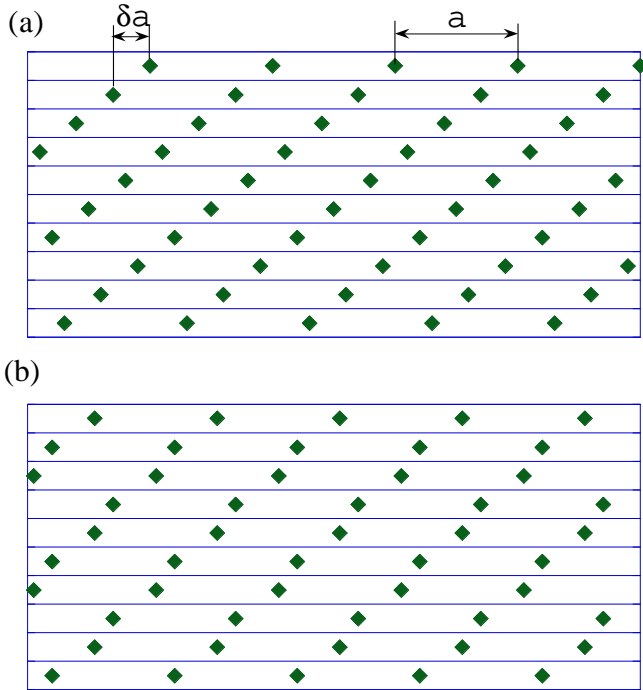


FIG. 1. Steady-states of moving Josephson lattice (squares mark positions where the interlayer phase difference is equal to $\pi + 2\pi m$): (a) a periodic lattice, the structure is determined by the lattice wave vector κ , which is connected with the shift between the lattices in the neighboring layers δa by relation $\kappa = 2\pi\delta a/a$ (b) a double-periodic lattice

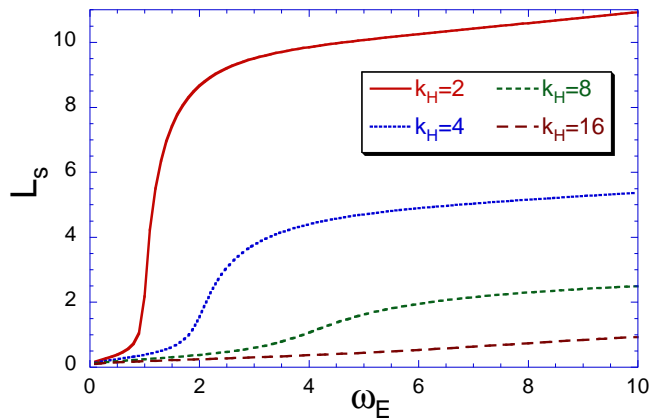


FIG. 2. The frequency dependence of the decay length L_s for different values of the magnetic wave vector k_H (see Table 1) for the typical parameters $\nu_{ab} = 0.1$ and $\nu_c = 0.002$. This length determines the interaction range between the Josephson planar arrays in different layers. A finite stack, containing N junctions, shows bulk behavior if $N \gg L_s$.

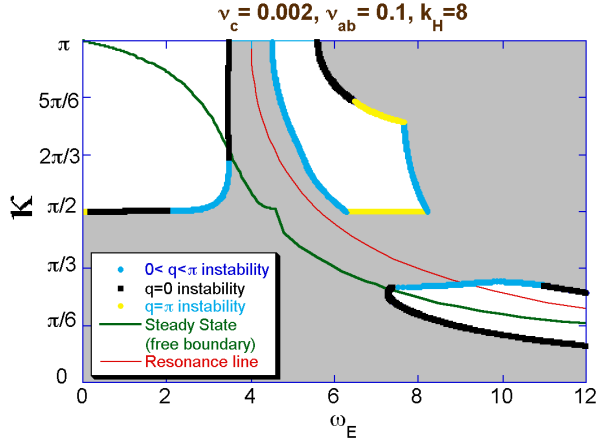


FIG. 3. Stability regions of the moving Josephson lattice in the plane ω_E - κ calculated for the representative parameters $\nu_c = 0.002$, $\nu_{ab} = 0.1$, and $k_H = 8$. Grey regions correspond to unstable lattices. Sections of boundaries marked by black correspond to the long-wave instability. Sections marked by light grey correspond to the short-wave instability. Line starting at $(0, \pi)$ shows dependence of the lattice wave vector on the frequency ω_E (lattice velocity) selected by the ideally reflecting boundary. We also show the resonance line, corresponding to matching between the Josephson frequency and the frequency of the plasma wave at the wave vector κ .

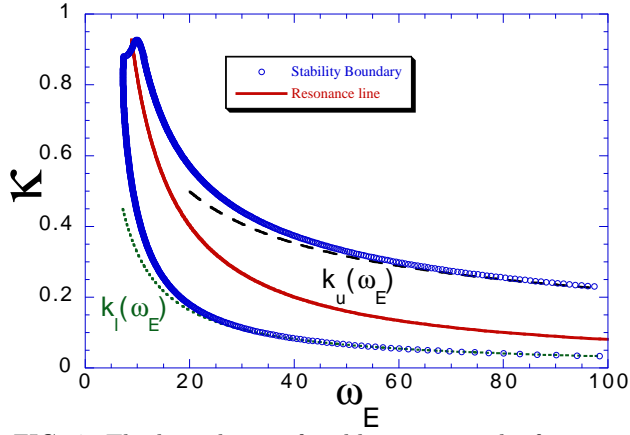


FIG. 4. The boundaries of stable region in the frequency range $k_H \ll \omega_E \ll k_H l$ for the same parameter set as in Fig. 3. The line in the middle is the resonance line. Dotted and dashed lines show the asymptotics of the lower and upper boundaries given by Eqs. (51) and (52).

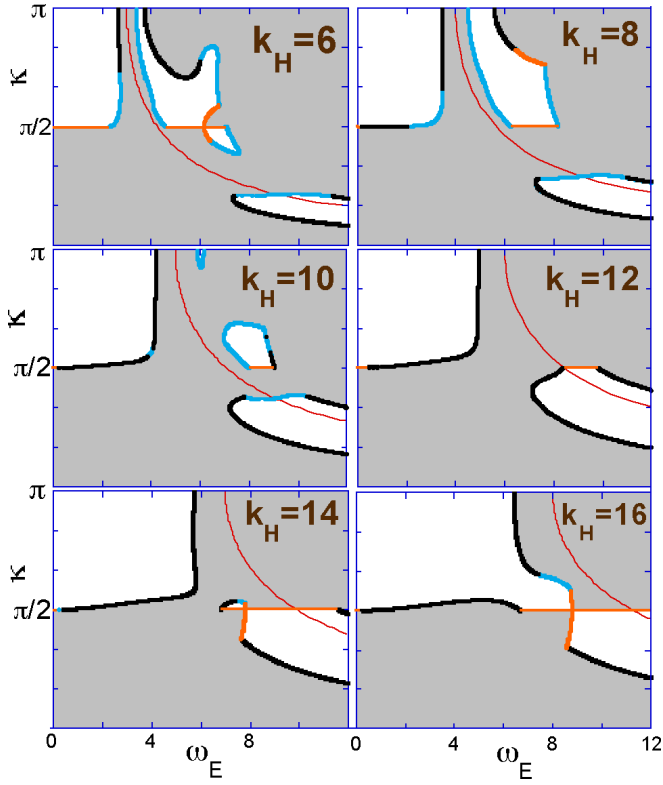


FIG. 5. Evolution of the stability diagram with increase of the magnetic field (for $\gamma = 500 H \approx k_H \cdot 0.3\text{T}$).

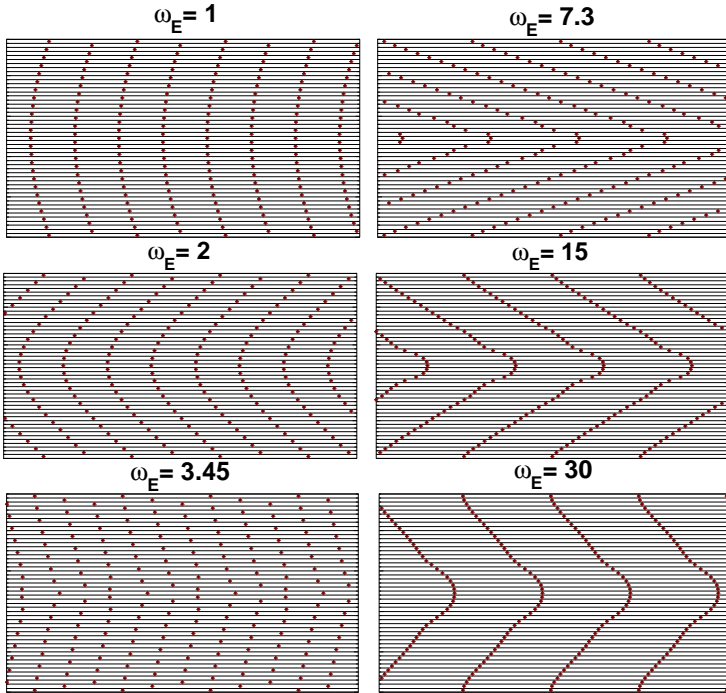


FIG. 6. Lattice structures in the real space at different values of the Josephson frequency ω_E (lattice velocity). The structures are generated using numerically calculated phase shifts for the system with 51 layers and the same parameters as in Fig. 3. ($\nu_c = 0.002$, $\nu_{ab} = 0.1$, and $k_H = 8$). The left column shows the lattice structures in the low-velocity stability region, below the first instability point. The right column shows the lattice structures in the high-velocity stability region.

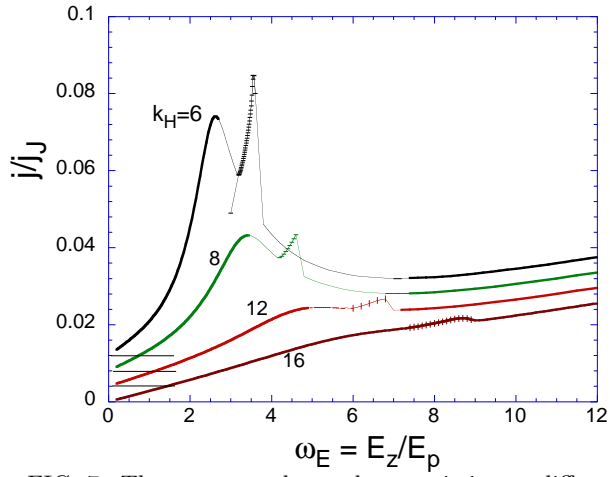


FIG. 7. The current-voltage characteristics at different magnetic fields, for $k_H = 6, 8, 12,$ and 16 . The dependencies are obtained using numerically computed steady-states with parameters $\nu_c = 0.002, \nu_{ab} = 0.1$. Thick lines show the stable branches and thin lines show the unstable branches. The branches, corresponding to the double-periodic states, are marked by dashes. The plots are displaced vertically for clarity.

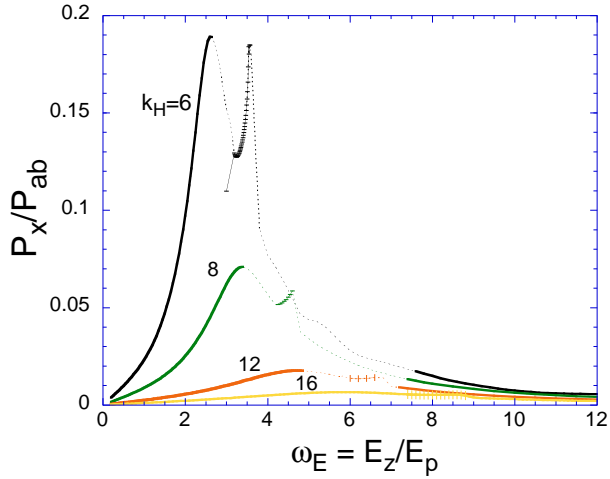


FIG. 8. Electric field dependencies of the Poynting vector along the layers for electromagnetic wave generated by the moving lattice (see Eq. (34)). The scale P_{ab} is defined by Eq. (36). We use the same notations for different branches as in the previous figure.

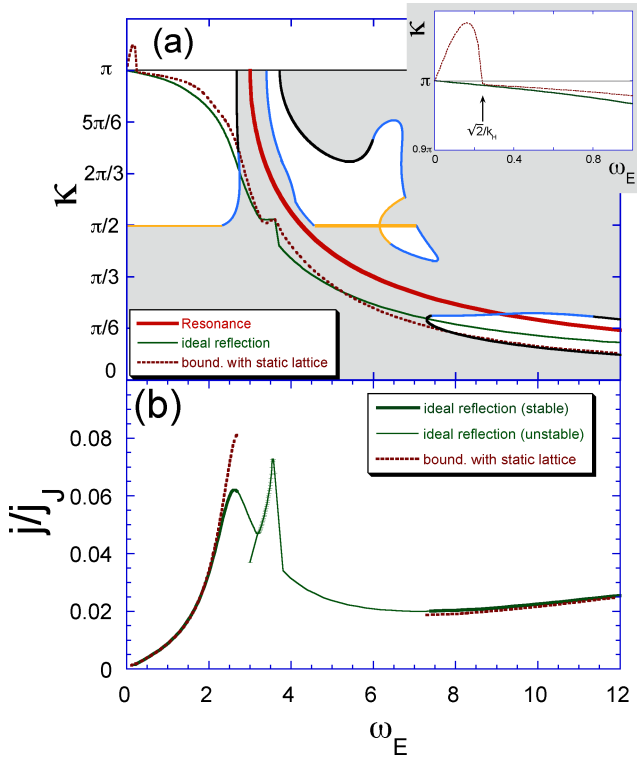


FIG. 9. This figure illustrates influence of the boundary conditions on the structure evolution (a) and the current-voltage dependence (b). We compare the ideally reflecting boundary ($\mathcal{B} = -1$) and the boundary with the static lattice ($\mathcal{B}(k, \omega)$ is calculated in Appendix D). The comparison is made for $\nu_c = 0.002$, $\nu_{ab} = 0.1$, and $k_H = 6$. Both cases show an overall similar behavior. In the second case there is a region at small Josephson frequencies, $0 < \omega < \sqrt{2}/k_H$, of the anomalous structure evolution, where the lattice wave vector exceeds π (this region is blown up in the inset). This region corresponds to the frequency range of the acoustic branch in the oscillation spectrum of the static Josephson lattice. The dependence $\kappa(\omega_E)$ has a kink at the endpoint of the spectrum. However this point is almost invisible in the I-V dependence. The second case is also characterized by the stronger current enhancement near the instability point (we show only stable I-V branches for this case).

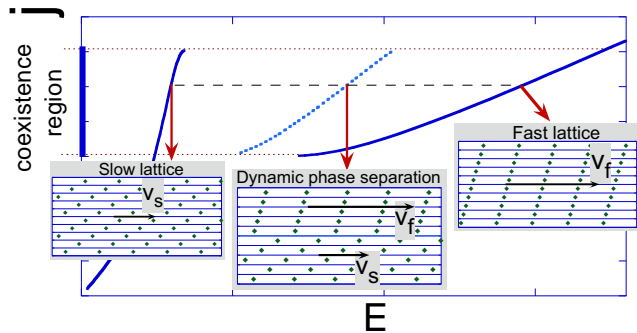


FIG. 10. Multibranch structure of the current-voltage characteristic due to the dynamic phase separation. Two states corresponding of the slow lattice motion (velocity v_s) and the fast lattice motion (velocity v_f) coexist within the current range marked at the vertical axis. In this region the intermediate phase-separated states exist, in which the system is split into the rapidly and slowly moving regions. The intermediate branch corresponding to one of such states is shown by dotted line.

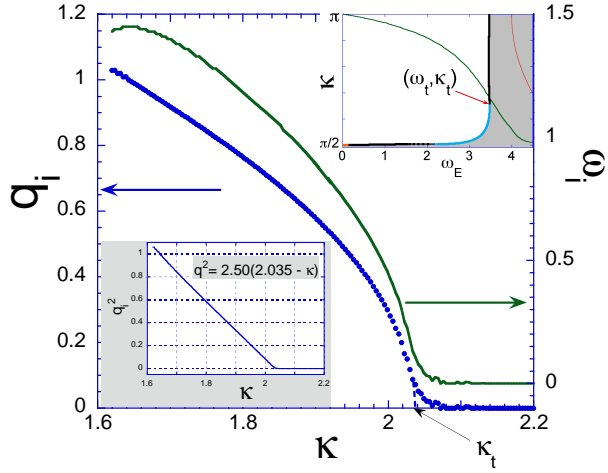


FIG. 11. Behavior of the wave vector q_i (left axis) and frequency $\omega_i = \text{Im}[\alpha(q_i)]$ (right axis) of the unstable mode. The upper-right inset shows the transition point in the κ - ω_E diagram of Fig. 3. Lower-left inset shows plot $q_i^2(\kappa)$ with linear fit below the transition.

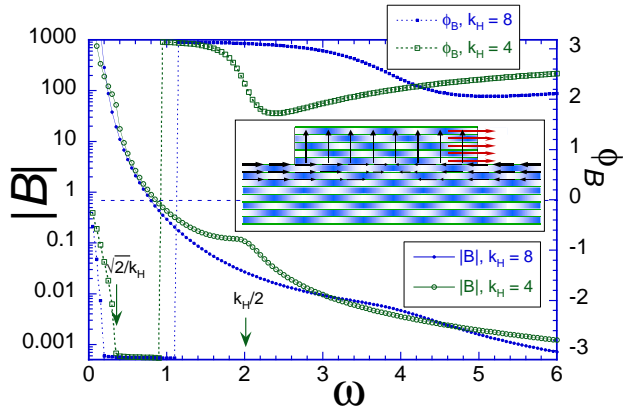


FIG. 12. The frequency dependence of the absolute value ($|B|$) and phase (ϕ_B) of the amplitude of reflected wave for the boundary between moving and static lattices (Eq. (77)). The plotted curves are computed using parameters $\nu_c = 0.002$, $\nu_{ab} = 0.1$ for two values of k_H , 4 and 8. The typical frequencies of the oscillation spectrum of the static lattice ($\omega = \sqrt{2}/k_H$ and $k_H/2$) are marked for $k_H = 4$. Inset sketches a small mesa on the top of bulk crystal. Concentration of the c -axis transport current inside the mesa forces the lattice move only in this region.